

Reviewed Preprint

v1 • May 28, 2026

Not revised

✉ For correspondence:

mtsuji@bs.s.u-tokyo.ac.jpemoto@bs.s.u-tokyo.ac.jp

Competing interests: No competing interests declared

Funding: See [page 18](#)

Reviewing editor: Hiromu Tanimoto, Tohoku University, Japan

© 2026, Tsuji et al. This article is distributed under the terms of the [Creative Commons Attribution License](#), which permits unrestricted use and redistribution provided that the original author and source are credited.

Dopaminergic Neurons Linking Threat Processing to Cardiac Modulation and Locomotor Responses

Masato Tsuji¹ ✉, Daisuke Jinkoma¹, Yuki Uemura¹, Ayako Ogasawara¹, Kazuo Emoto^{1,2} ✉

¹Department of Biological Sciences, Graduate School of Science, The University of Tokyo, Tokyo, Japan • ²International Research Center for Neurointelligence (WPI-IRCN), The University of Tokyo, Tokyo, Japan

eLife Assessment

This **important** study identifies two pairs of dopaminergic neurons (DA-WED) in *Drosophila* that coordinate cardiac deceleration and locomotor responses to a mechanical threat. The evidence is **convincing**, supported by comprehensive optogenetic, physiological, and behavioral experiments showing that these neurons are required for and sufficient to drive threat-associated cardiac slowing. The proposed role of cardiac deceleration as an interoceptive contributor to locomotion is intriguing, but should be presented more cautiously, as the causal relationship between heartbeat changes and locomotor output remains less directly established. The work will be of broad interest to those interested in neural circuits, neuromodulation, and the integration of physiological and behavioral responses.

<https://doi.org/10.7554/eLife.111256.1.sa3>

Abstract

Heartbeat and behavior are tightly coordinated during defensive states, yet the neuronal mechanisms linking threat processing to cardiac modulation—and the potential contribution of cardiac dynamics to behavioral output—remain poorly understood. Here we show in *Drosophila* that mechanical threat triggers locomotion together with cardiac deceleration. We identify two dopaminergic neurons, termed DA-WED neurons, that mediate this cardiac response: silencing these neurons markedly attenuates threat-induced cardiac deceleration, whereas optogenetic activation induces cardiac deceleration in the absence of threat. Calcium imaging further shows that DA-WED neurons are activated by mechanical threat. Linking cardiac dynamics to behavior, direct optogenetic manipulation of cardiomyocytes that quantitatively reproduces threat-evoked cardiac deceleration is accompanied by increased locomotion. Together, these results identify a dopaminergic descending pathway that links threat processing to cardiac modulation and suggest that cardiac dynamics may contribute to shaping defensive behavior.

Introduction

Heartbeat dynamics are tightly coordinated with behavioral state. Defensive states, for example, are accompanied by coordinated modulation of cardiac activity, including transient cardiac deceleration during threat detection and cardiac acceleration during active coping in mammals¹. Such tight coordination between behavioral state and cardiac dynamics is likely advantageous for survival: cardiac deceleration may minimize the brain-wide representations of the heartbeat^{2–5} to sharpen sensory processing¹⁶, whereas cardiac acceleration boosts the delivery of metabolic resources to muscles⁷. Although much of the existing work on heart–behavior coupling has focused on mammals, comparable threat-associated cardiac modulation has also been reported in invertebrates. In decapod crustaceans, for instance, sensory stimuli elicit time-locked heart rate changes that parallel defensive behaviors, suggesting that coordinated heart–behavior responses

are evolutionarily widespread^{8,9}. Despite this well-documented coupling, the circuit mechanisms linking threat processing in the brain to cardiac modulation—and whether cardiac dynamics contribute to behavioral output—remain incompletely understood.

In mammals, heartbeat is governed by sympathetic and parasympathetic branches of the autonomic nervous system (ANS) that innervate the heart^{7,10–17}. Sympathetic output that accelerates the heartbeat arises from brainstem and hypothalamic circuits and projects through spinal intermediates to the heart⁷. On the other hand, the parasympathetic nervous system, which decelerates the heartbeat^{7,18}, originates from the dorsal motor nucleus of the vagus nerve and nucleus ambiguus, and projects directly to the heart^{18,19}. These autonomic pathways are engaged in threatened animals by the so-called fear circuitry in the brain^{20–22} to shape cardiac responses, typically producing cardiac deceleration followed by acceleration^{1,23–28}. Circuit-wise, the periaqueductal gray (PAG) is considered the output hub of the fear circuitry and modulates the heartbeat through the hypothalamus, midbrain, pons, and medulla oblongata²⁹. In addition, hypothalamic nuclei such as the dorsomedial hypothalamus (DMH)³⁰ and the arcuate nucleus (ARC), as well as the anterior cingulate cortex (ACC)³¹, also modulate the heartbeat upon threats^{32–38}.

In parallel, ascending feedback from the heart to the brain has attracted increasing attention. Such interoceptive signaling³⁹ is conveyed by sensory neurons innervating the heart and aortic arch³⁹, which project to NTS and onward to hypothalamic and cortical regions including paraventricular nucleus of the hypothalamus (PVN)⁴⁰, ACC, insular, and prefrontal cortex⁴⁰. These pathways have been implicated in learned fear⁴¹, anxiety-like behavior⁴² or sleep⁴³. Together, these findings suggest that bidirectional communication between brain and heart may shape physiological and behavioral responses during defensive states. However, how central circuits orchestrate threat-associated cardiac modulation, and whether cardiac dynamics influence defensive behavior, remain unresolved.

The fruit fly *Drosophila melanogaster* provides a genetically tractable system to dissect brain–body interactions. The *Drosophila* heart, an evolutionarily conserved organ^{44–47}, consists of two rows of cardiomyocytes forming a tubular structure that runs through the midline of the abdomen^{48,49}. Like mammalian heart, *Drosophila* heart receives rich neuronal projections throughout^{50,51}. Recent work has shown that visual threat induces cardiac deceleration in *Drosophila*⁵², suggesting the existence of the neuronal mechanism in the brain that modulates the heart. However, the neuronal substrate of such a mechanism, and the behavioral consequences of cardiac modulation during threat, remain largely unknown.

We have recently reported that a train of air puffs elicit hyperactivity, avoidance of puffs, and aversion from an otherwise neutral visual object, suggesting that air puffs serve as mechanical threat⁵³. Building on this work, we established an experimental paradigm to assess how mechanical threat modulates heartbeat and behavior. Using this system, we identify two pairs of dopaminergic neurons in the brain, termed DA-WED neurons, that are responsible for threat-induced cardiac deceleration. We further examine how cardiac deceleration relates to threat-induced locomotion. Together, our findings identify a pair of dopaminergic neurons that link threat processing in the brain to cardiac modulation and suggest that cardiac dynamics may contribute to shaping defensive behavior.

Results

I. Air puffs induce cardiac deceleration and locomotion

We have previously reported that a train of air puffs serve as mechanical threats, eliciting a host of fear-like behaviors such as hyperactivity, avoidance of puffs, and aversion from an otherwise neutral visual object⁵³. This motivated us to test how the air puff might influence heartbeat, and its relation to behavior. For this purpose, we developed a paradigm to monitor heartbeat and behavior simultaneously (Fig. 1a [↗](#)). Our paradigm images the heart chamber closest to the thorax, called conical chamber, which is visualized through the dorsal cuticle by cuticle-penetrating infare-red light (Fig. 1a [↗](#), “CAM1”). Simultaneously, the fly’s behavior is recorded

from the side of the fly (Fig. 1a [↗](#), “CAM2”). We further developed a set of software to automatically detect heartbeat and behavior (Supplementary Movie 1 [↗](#)). Our heartbeat detection software takes two consecutive frames and calculates for each pixel the optical flow, which are used to quantify the overall relaxation (diastole) or shrinkage (systole) of the heart (Supplementary Fig. 1a-c [↗](#)). Based on such quantification, our software detects the timings at which the heart was shrunk most (systole peak), which were counted to obtain the heart rate (HR). Our analysis pipeline for behavior detection first tracks the coordinate of body parts (joints of each leg, eye, neck, haltere, rostral tip of the abdomen, all on the right side of the fly), utilizing SLEAP software⁵⁴. The tracked coordinates are then fed into our custom support vector machine-based program to detect locomotion. Our analysis pipeline allowed us to visualize the HR and locomotion over time in a synchronized fashion.

Using our paradigm, we tested how the air puff might influence the HR and locomotion. Specifically, we applied for each fly a 0.5 s air puff (either 20 mL/min, 50 mL/min, 200 mL/min). We repeated 10 trials for each fly with an inter-puff interval of 90s (Fig. 1b [↗](#)). The results of 10 trials were averaged, as we did not observe noticeable trial effects (Supplementary Fig. 2a, c [↗](#)). We found that the air puff transiently decreased the HR (Fig. 1c-e [↗](#); Supplementary Fig. 2a, b [↗](#); Supplementary Movie 1 [↗](#)). Similar tendency was observed but was statistically insignificant for the strongest puff (200 mL/min), which is likely due to the following cardiac acceleration (Fig. 1d, e [↗](#)). Surgical removal of body parts and silencing experiments of external sensilla or chordotonal organ^{55,56} suggest that hair plate neurons and chordotonal organs are at least partially indispensable for puff-induced cardiac deceleration (Supplementary Fig. 3 [↗](#)). We also found that the air puff persistently increased the fraction of time walking, in line with previous reports (Fig. 1f, g [↗](#); Supplementary Fig. 2c, d [↗](#))^{53,57}. Thus, our data revealed that the air puff induces cardiac deceleration and locomotion. Notably, in our paradigm the air puff robustly induces locomotion and does not elicit sustained freezing, indicating that the observed cardiac deceleration cannot be attributed to freezing-associated bradycardia described in visually induced threat paradigms in flies⁵² or in other contexts in rodents¹. This prompted us to next identify neurons responsible for cardiac deceleration.

II. Dopaminergic system is responsible for puff-induced cardiac deceleration

To aid in identifying neurons responsible for cardiac deceleration, we developed yet another paradigm to quantify the HR with higher throughput. In this paradigm, we drove the expression of GFP in the cardiomyocytes using the enhancer of the Hand gene⁴⁵, to aid in heartbeat imaging (Fig. 2a, b [↗](#)). GFP signals in pericardiocytes (also known as nephrocytes) are likely due to their function to incorporate any molecules in the hemolymph⁵⁸. The fly's ventral side of the thorax and abdomen were glued to a slide glass, and the GFP signals in the conical chamber were acquired through the intact dorsal cuticle by confocal microscopy (Fig. 2a, b [↗](#)). The air puffs of 20 mL/min were applied frontally to the fly's head through a glass pipette (Fig. 2a [↗](#)). Heartbeat was detected using our custom software (Supplementary Fig. 4a-c [↗](#)). A single trial consisted of 60 s of interval, 10 s of air puffs, and 60 s of recording, which was repeated twice for each fly with 90s interval (Fig. 2c [↗](#)). This experiment revealed that air puffs induce cardiac deceleration by roughly 10% (Fig. 2d-f [↗](#); Supplementary Movie 2 [↗](#)), consistent with our earlier finding (Fig. 1 [↗](#)). Similar results were obtained when the air puff was applied for 1s (Supplementary Fig. 4d, e [↗](#)), 20s (Supplementary Fig. 4f, g [↗](#)), and in both sexes (Supplementary Fig. 4h, i [↗](#)).

Monoaminergic systems have repeatedly been implicated in HR regulation across species, including *Drosophila*^{59–68}. We thus wondered whether monoaminergic systems might be involved in puff-induced cardiac deceleration. When we silenced with TNT the neurons expressing either serotonin, octopamine (insect equivalent of norepinephrine), and dopamine, we found that silencing of octopaminergic or dopaminergic neurons significantly suppressed puff-induced cardiac deceleration (Fig. 2g, h [↗](#); Supplementary Fig. 5a, b [↗](#)). Note, however, that when we expressed in serotonin neurons the inward-rectifying potassium channel Kir2.1, it did decrease the puff-induced cardiac deceleration (Supplementary Fig. 5c, d [↗](#)), suggesting that serotonergic

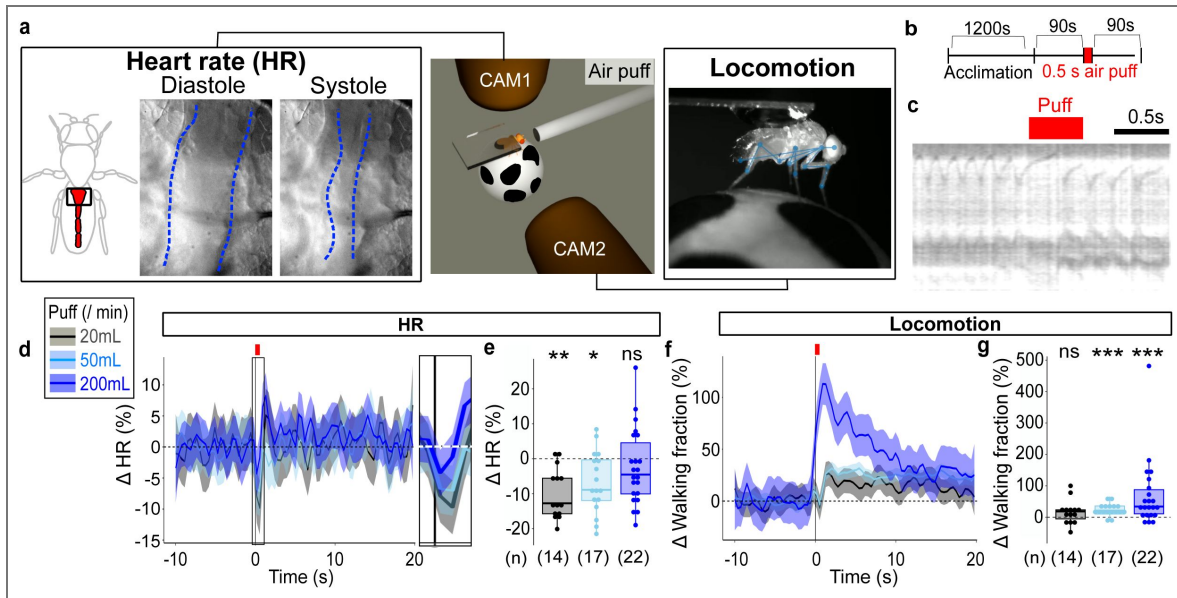


Fig. 1. Mechanical threat induces cardiac deceleration and locomotion

Schematics of the paradigm. The fly is fixed on an air-supported ball. Left: the heart rate (HR) was videotaped by an IR-sensitive camera from the dorsal side through the cuticle (“CAM1”). Of the four cardiac chambers, our system videotaped the chamber closest to the thorax called conical chamber. We could easily distinguish diastole and systole in the captured video (blue dashed lines indicate the heart wall). Right: simultaneously, locomotion was videotaped from the right side of the fly (“CAM2”). Blue dots and lines indicate automatically tracked body parts. The time course of the experiment. An air puffs of 0.5 s was applied once. The trial was repeated 10 times for each fly, the results of which were averaged. **c.** An example M-mode of the heartbeat. An air puff was applied during the red-shaded time window. **d.** Time course of the HR (% change from baseline defined as the average during the 10 s preceding puff onset). N = 14, 17, 22 for 20mL/min (gray), 50mL/min (sky blue), and 200mL/min (dark blue), respectively. The inset shows the magnified view of the cardiac deceleration indicated by the box. **e.** Change in HR, calculated for each fly as the % difference between the mean fraction during the 1 s following stimulation onset and the mean fraction during the 10 s baseline period preceding stimulation. N = 14, 17, 22 for 20mL/min (gray), 50mL/min (sky blue), and 200mL/min (dark blue), respectively. ******p < 0.01, *****p < 0.05, n.s.: p > 0.05, Wilcoxon’s signed rank test followed by Bonfferoni correction. **f.** Time course of the walking fraction (% change from baseline defined as the mean fraction during the 10 s preceding puff onset). N = 14, 17, 22 for 20mL/min (gray), 50mL/min (sky blue), and 200mL/min (dark blue), respectively. *******p < 0.001, n.s.: p > 0.05, Wilcoxon’s signed rank test followed by Bonfferoni correction. **g.** Change in walking fraction, calculated for each fly as the % difference between the mean fraction during the 10 s following stimulation onset and the mean fraction during the 10 s baseline period preceding stimulation. N = 14, 17, 22 for 20mL/min (gray), 50mL/min (sky blue), and 200mL/min (dark blue), respectively. *******p < 0.001, n.s.: p > 0.05, Wilcoxon’s signed rank test followed by Bonfferoni correction.

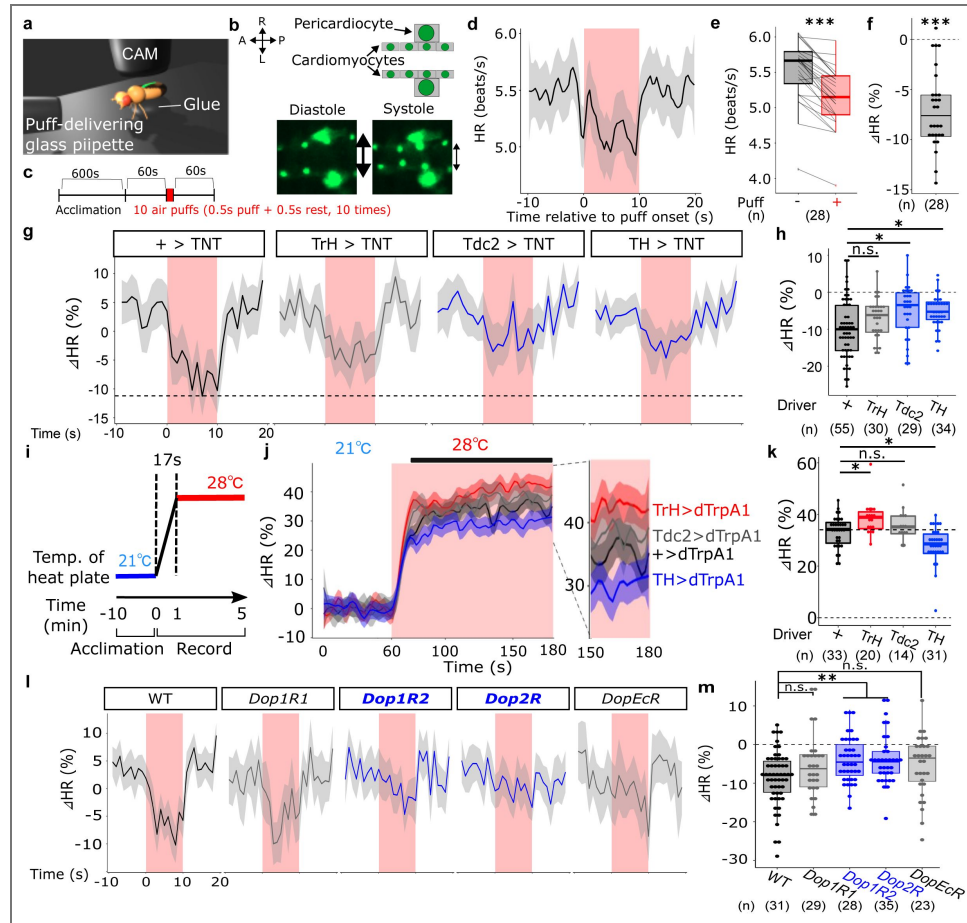


Fig. 2. Dopamine system is responsible for puff-induced cardiac deceleration

a. Experimental setup. Hand enhancer drives the GFP expression in the cardiomyocytes (and in pericardiocytes). The fly was glued onto a slide glass, and the GFP signals were acquired through the intact cuticle. The air puffs were applied frontally to the fly's head. **b.** Example heartbeat. (Upper) Cartoon of the acquired image. Two rows of small cardiomyocytes and one pair of large pericardiocytes are visible. (Lower) Diastole and systole can be distinguished by the changing distance between two rows of cardiomyocytes (arrows). **c.** The time course of the experiment. Air puffs of 0.5 s were applied at 1 Hz for 10 times (totalling 10 s). The trial was repeated twice for each fly, the results of which were averaged. **d.** Time course of the HR. Air puffs are applied during red-shaded window. Lines and shaded areas represent means and SEM, respectively. N = 28. **e.** The HR averaged during puff application window ("puff +") vs 10 s before puff application ("puff -"). Each line corresponds to each fly. N = 28, ***p < 0.001, two-tailed t-test. **f.** Difference between puff+ HR and puff- HR, calculated for each fly. N = 28, ***p < 0.001, two-tailed t-test. **g.** Time course of the HR (% change from baseline defined as the average during the 10 s preceding puff onset). Air puffs were applied during the red-shaded time window. Lines and shaded areas represent means and SEM, respectively. TNT expression is driven by indicated drivers. "+" indicates driver-less control. Dashed line shows the lowest mean of "+" control during puffs. N = 55, 30, 29, 34, for +, TrH, Tdc2, TH, respectively. **h.** Change in HR, calculated for each fly as the % difference between the mean HR during the 10 s stimulation period and the mean HR during the 10 s baseline period preceding stimulation. N = 55, 30, 29, 34, for +, TrH, Tdc2, TH, respectively. *p < 0.05, n.s.: p > 0.05, Dunn's test. **i.** Time course of the experiment. The heat plate beneath the slide glass warmed up the fly. The temperature of the slide glass is held at 21°C for 10 min and ramped up to 28°C for 5 min. Note it took approximately 17 s for the temperature to ramp from 21°C to 28°C. **j.** Time course of the HR, shown as % change from average HR at 21°C. Temperature was ramped from 21°C to 28°C during red-shaded window. **k.** % Changes in the HR (28°C vs 21°C) from the baseline (average over initial 60 s) averaged over 75s - 180s window (shown as black bar in j). N = 33, 20, 14, 31, for +, TrH, Tdc2, TH, respectively. *p < 0.05, n.s.: p > 0.05, Dunn's test. The upper dashed line shows the median of "+" control. **l.** Time course of the HR (% change from baseline defined as the average during the 10 s preceding puff onset). Air puffs were applied during the red-shaded time window. Lines and shaded areas represent means and SEM, respectively. N = 31, 29, 28, 35, 23, for +, WT, *Dop1R1*, *Dop1R2*, *Dop2R*, *DopEcR*, respectively. **m.** Change in HR, calculated for each fly as the % difference between the mean HR during the 10 s stimulation period and the HR HR during the 10 s baseline period preceding stimulation. N = 31, 29, 28, 35, 23, for +, WT, *Dop1R1*, *Dop1R2*, *Dop2R*, *DopEcR*,

neurons may also be indispensable for puff-induced cardiac deceleration. In line with this, a *loss-of-function* mutation of a serotonin synthetic enzyme *TrH* also showed decrease in the puff-induced cardiac deceleration (Supplementary Fig. 5e-g).

To further probe the roles of monoaminergic neurons, we next tested whether thermogenetic activation of these neurons can induce cardiac deceleration without air puffs. To this end, we expressed a heat-gated cation channel dTrpA1 in monoaminergic neurons, and shifted the temperature from 21°C to 28°C while monitoring the HR (Fig. 2i). This revealed that, while the HR of cold-blooded *Drosophila* increased as a function the temperature even in the driver-less control (Fig. 2j, black), such cardiac acceleration was suppressed by activation of dopaminergic neurons (Fig. 2j, blue) but not by octopaminergic neurons (Fig. 2j, gray). On the other hand, activation of serotonergic neurons exaggerated the heat-induced cardiac acceleration (Fig. 2j, red). The average HR during 28°C period indeed revealed that the activation of dopaminergic neurons significantly decreased the HR compared to the driver-less control, while the activation of serotonergic neurons significantly increased the HR (Fig. 2k). Dopaminergic neurons were the only monoaminergic population whose silencing and activation consistently implicated them in driving cardiac deceleration (Fig. 2g-k). The role of dopaminergic neurons is further reinforced by loss-of-function experiments of dopamine receptors, which revealed that mutations of *Dop1R2* or *Dop2R* significantly decrease the puff-induced cardiac deceleration (Fig. 2l, m; Supplementary Fig. 5h, i). A mutation of *DopEcR* also showed a tendency to decrease the puff-induced cardiac deceleration albeit not quite reaching the statistical significance (Fig. 2l, m; Supplementary Fig. 5h, i). Together, our data demonstrates that dopamine system is responsible for puff-induced cardiac deceleration.

III. Two pairs of dopaminergic neurons in the brain, DA-WED neurons, are indispensable for cardiac deceleration

There are approximately 130 dopaminergic neurons scattered throughout the *Drosophila* brain^{69,70}. To identify the subpopulation of dopaminergic neurons responsible for puff-induced cardiac deceleration, we turned to a host of dopamine-related GAL4 driver lines⁶⁹ (Fig. 3a). Each of these drivers carries different bits of enhancers of dopamine-related genes, and presumably for this reason these drivers are known to label partially overlapping but distinct subpopulations of dopaminergic neurons⁶⁹. When we drove the expression of TNT by these drivers, we found that neuronal silencing by 4 out of 10 drivers decreased puff-induced cardiac deceleration (R76F01-, R76F02-, R76F05-, R60F07-GAL4; Fig. 3b, blue plots) without significantly influencing the baseline HR (Supplementary Fig. 6a), suggesting that these drivers label the subset of dopaminergic neurons indispensable for puff-induced cardiac deceleration. Identification of these “hit” drivers allowed us to next employ a split-GAL4 approach to further narrow down the indispensable neurons (Fig. 3c). In the split-GAL4 method, the whole GAL4 protein is split into the DNA-binding domain (“DBD”) and the activation domain (“AD”), each fused with a leucine-zipper domain⁷¹. When these “hemi-drivers” collide, they bind to each other through their respective leucine zipper, re-constituting the functional GAL4. Thus, by placing each of these hemi-drivers under different enhancers, one can achieve the expression of functional GAL4 only in cells in which both enhancers are active (Fig. 3c). When we tested all split combinations of the 4 “hit” enhancers, we found that only one combination, namely R76F05-DBD and R60F07-AD, significantly decreased the puff-induced cardiac deceleration (Fig. 3d), without significantly influencing the baseline HR (Supplementary Fig. 6b). Our immunohistochemical analysis revealed that, as reported by a previous report⁶⁹, the split combination of R76F05-DBD and R60F07-AD labeled two different subpopulations of dopaminergic neurons: one subpopulation from the PPL1 cluster named PPL1-SMPy, and another subpopulation from the PPM2 cluster named DA-WED (Fig. 3e), with additional one or two neurons occasionally labeled in some brains. We further sought to identify which of these two subpopulations is indispensable for puff-induced cardiac deceleration. Taking advantage of the recently-developed analysis pipeline that identify a list of candidate GAL4 drivers that may label any neuron of interest^{72,73}, we obtained a list of candidate PPL1-SMPy and DA-WED drivers. By testing several split combinations of enhancers used in these drivers, we

could identify the split combinations that label one but not the other (Fig. 3f). We note that each of these combinations labels additional neurons, in either subesophageal zone (Fig. 3f, left) or optic lobes (Fig. 3f, right). Using these split drivers, we silenced either PPL1-SMPy or DA-WED with TNT, and found that silencing of DA-WED significantly decreased puff-induced cardiac deceleration (Fig. 3g; Supplementary Fig. 6c). Together, our data suggests that DA-WED neurons are indispensable for puff-induced cardiac deceleration.

IV. DA-WED neurons are responsible for puff-induced cardiac deceleration

While our data so far suggests the role of DA-WED neurons in cardiac deceleration, the split driver we used to label DA-WED also labeled neurons in the optic lobes (Fig. 3f, right). We thus further improved the labeling specificity through intersection strategy.

In this strategy, the effector gene is expressed under the control of UAS sequence, but a “stop” sequence is inserted in between UAS and GFP, blocking the function of GAL4. Now, the expression of “molecular scissors” called flippase (FLP) is driven by a Tyrosine hydroxylase (TH) promoter (“TH-FLP”), which excises out the stop sequence. Hence, GAL4 can function only in cells in which TH promoter is active. This strategy, combined with our split GAL4 combination, indeed achieved near-perfect specificity for DA-WED neurons, apparently labeling no other cells throughout the body (Fig. 4a; Supplementary Fig. 6d). When we silenced DA-WED neurons with Kir2.1, it decreased puff-induced cardiac deceleration (Fig. 4b, c), without noticeably influencing the baseline HR (Supplementary Fig. 6e).

We next tested if DA-WED neurons function through dopamine. Our dopamine receptor mutant analysis (Fig. 2l, m) suggests that dopamine signaling through Dop1R2 and Dop2R is indispensable for cardiac deceleration. Consistent with this, we found that RNAi of a dopamine synthesis enzyme *ple* in DA-WED neurons reduced puff-induced cardiac deceleration (Supplementary Fig. 6f-h). It is thus plausible that DA released from DA-WED neurons binds to Dop1R2 and/or Dop2R to drive cardiac deceleration.

DA-WED neurons have previously been reported to drive protein preference behavior in protein-deprived flies^{74,75}. Indeed, suppression of DA-WED neurons decreased protein preference (Supplementary Fig. 7a-d)^{74,75} in addition to cardiac deceleration (Supplementary Fig. 7e, Fig. 4b, c). This prompted us to ask whether these neurons drive cardiac deceleration and protein preference through shared, or instead distinct, mechanisms. Interestingly, *Dop2R* mutant flies failed to show cardiac deceleration (Fig. 2l, m), but showed normal preference compared to the wildtype (Supplementary Fig. 7f, g). Similarly, suppression of FB-LAL neurons, through which DA-WED neurons drive protein preference^{74,75}, failed to influence cardiac deceleration (Supplementary Fig. 7h, i). These results suggest that DA-WED neurons drive protein preference through FB-LAL neurons, while driving cardiac deceleration through Dop2R independent of FB-LAL. This hypothesis is further reinforced by our observations that protein deprivation, which drives protein preference (Supplementary Fig. 7j), fails to influence puff-induced cardiac deceleration (Supplementary Fig. 7k) nor the baseline HR (Supplementary Fig. 7l). Together, our data suggests that DA-WED neurons drive cardiac deceleration and protein preference through distinct mechanisms (Supplementary Fig. 7m).

We next wondered how DA-WED neurons might respond to air puffs. To this end, we expressed jGCaMP7s in DA-WED neurons, and imaged their calcium activities while applying a train of air puffs (Fig. 4d). We found that the calcium level of DA-WED neurons steadily increased as air puffs are applied (Fig. 4e, f; Supplementary Fig. 8a; Supplementary Movie 3). The increased jGCaMP7s signals returned to the baseline in less than 5 s when puffs ceased (Fig. 4f). Given the slow kinetics of jGCaMP7s⁷⁶, the increased activity of DA-WED neurons likely returns to the baseline immediately when the puffs cease. While there are two pairs of DA-WED neurons in the brain, one pair being more medial than the other, we found no noticeable difference in medial vs lateral DA-WED neurons' activities in response to puffs (Supplementary Fig. 8b-d). Our data suggests that all four DA-WED neurons transiently get activated by air puffs.

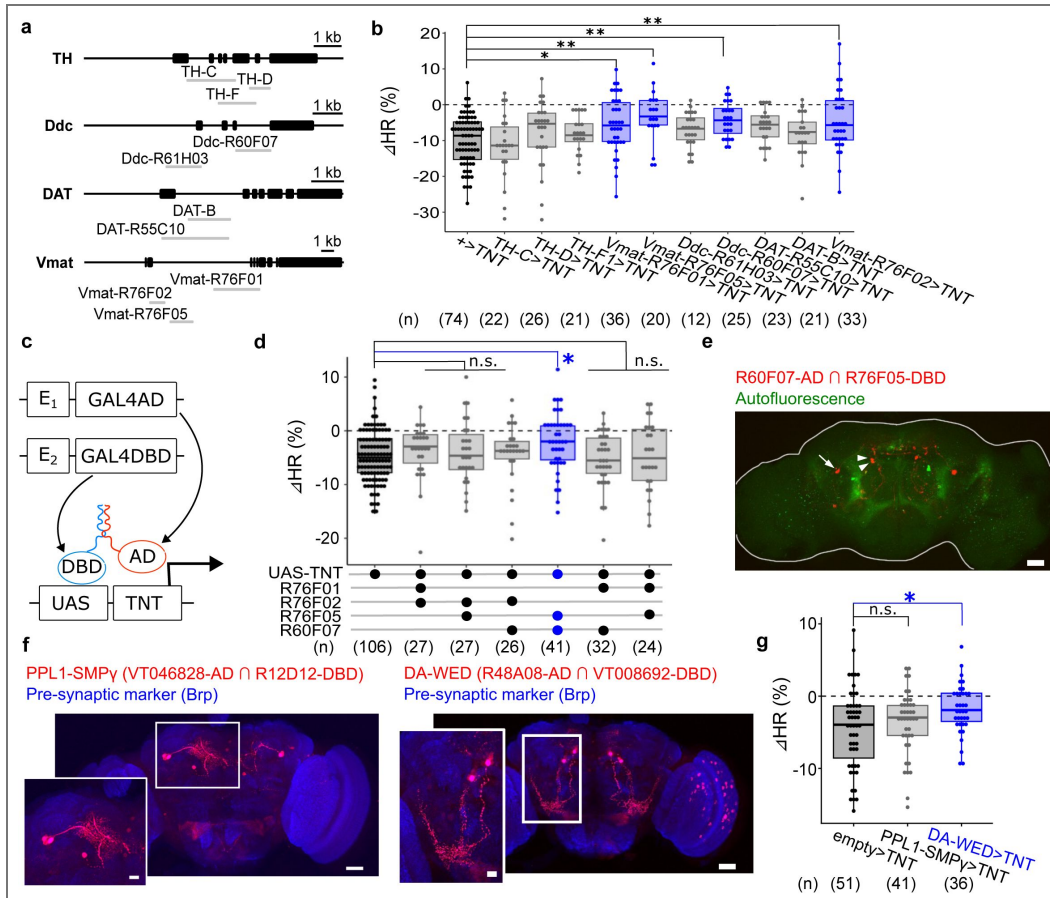


Fig. 3. Two pairs of dopaminergic neurons in the brain are partially indispensable for cardiac deceleration

a. AsSchematic of different DA-related GAL4 drivers. **b.** Change in HR, calculated for each fly as the % difference between the mean HR during the 10 s stimulation period and the HR HR during the 10 s baseline period preceding stimulation. N = 74, 22, 26, 21, 36, 20, 12, 25, 23, for +, TH-C, TH-D, TH-F1, Vmat-R76F01, Vmat-R76F05, Ddc-R61H03, Ddc-R60F07, DAT-R55C10, respectively. ** $p < 0.01$, * $p < 0.05$, n.s. (data shown in gray): $p > 0.05$, Dunnett's test. **c.** A schematic of split-GAL4 strategy. **d.** Change in HR, calculated for each fly as the % difference between the mean HR during the 10 s stimulation period and the HR HR during the 10 s baseline period preceding stimulation. N = 106, 27, 27, 26, 41, 32, 24, for driver-less control, R76F01 \cap R76F02, R76F02 \cap R76F05, R76F01 \cap R76F02, R76F02 \cap R76F07, R76F05 \cap R60F07, R76F01 \cap R60F07, R76F01 \cap R76F05, respectively. * $p < 0.05$, n.s.: $p > 0.05$, Dunn's test. **e.** Brain of R60F07-AD \cap R76F01-DBD>mCherry (red). An arrow indicates the soma of PPL1-SMP γ , while arrowheads indicate the soma of DA-WED. Scale bar: 25 μ m. Similar results were obtained across 3 independent samples. **f.** Brains of VT046828-AD \cap R12D12-DBD>mCherry and R48A08-AD \cap VT008692-DBD>mCherry (red) immunostained with anti-neuropil marker nc82 (blue). Scale bars: 25 μ m (inlet: 5 μ m). Similar results were obtained across 5 independent samples for each genotype. **g.** Change in HR, calculated for each fly as the % difference between the mean HR during the 10 s stimulation period and the HR HR during the 10 s baseline period preceding stimulation. N = 51, 41, 36 for empty>TNT, PPL1-SMP γ >TNT, DA-WED>TNT, respectively. * $p < 0.05$, n.s.: $p > 0.05$, Dunnett's test.

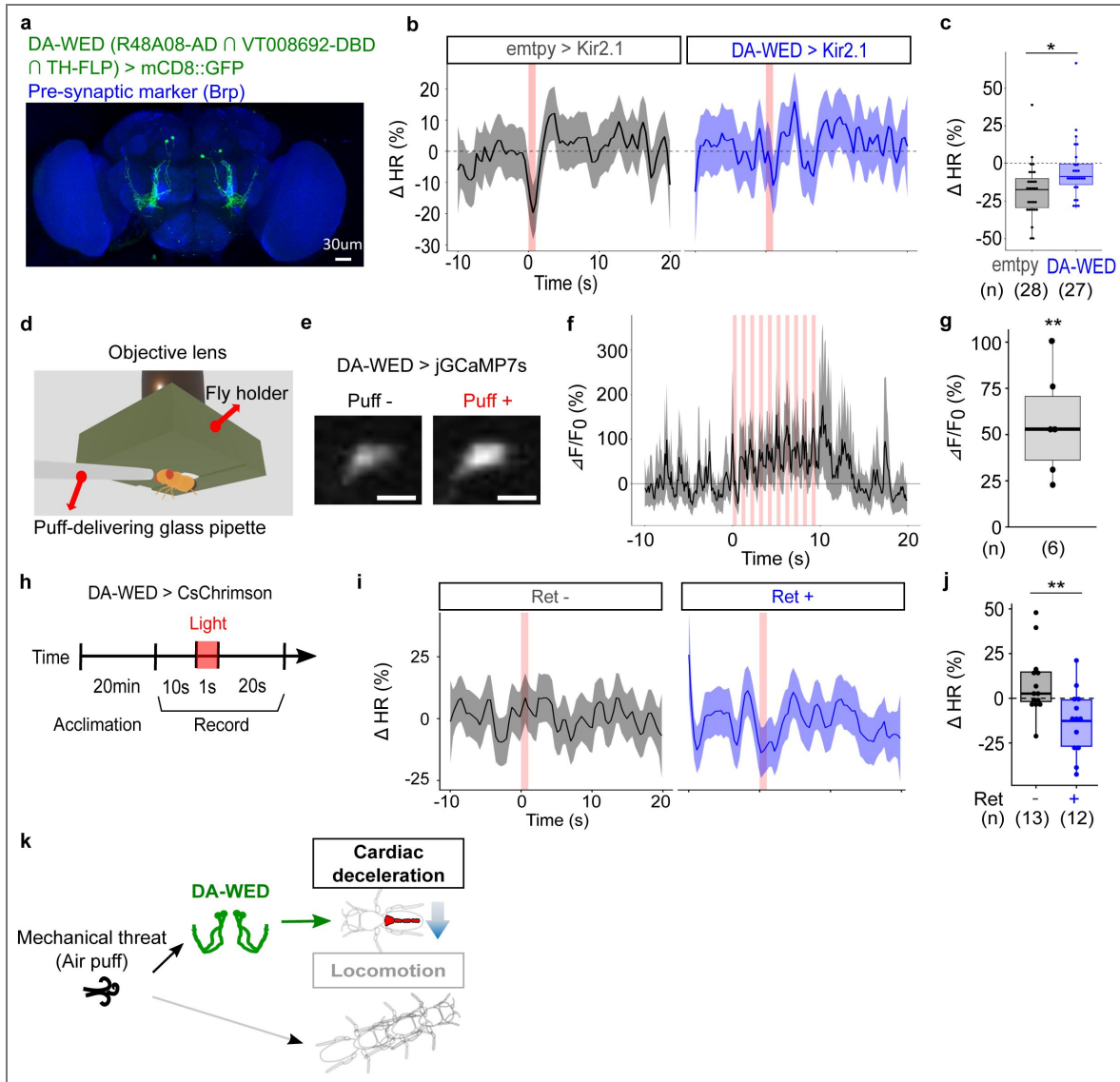


Fig. 4. DA-WED neurons are responsible for puff-induced cardiac deceleration

a. The brain of R48A08-AD \cap VT008692-DBD \cap TH-FLP>mCD8::GFP (green) immunostained with anti-neuropil marker nc82 (blue). Scale bar: 30 μ m. Similar results were obtained across 5 independent samples. **b.** Time course of the HR (% change from baseline defined as the average during the 10 s preceding puff onset). Air puff was applied during the red-shaded time window. Lines and shaded areas represent means and SEM, respectively. N = 28, 27, for empty>Kir2.1, DA-WED>Kir2.1, respectively. **c.** Change in HR, calculated for each fly as the % difference between the mean HR during the 1 s following stimulation onset and the mean HR during the 10 s baseline period preceding stimulation. N = 28, 27, for empty>Kir2.1, DA-WED>Kir2.1, respectively. * $p < 0.05$, Two-tailed t -test. **d.** Experimental setup. **e.** Representative images of DA-WED neurons expressing GCaMP7s before and during puff application. Scale bar: 5 μ m. **f.** Time course of $\Delta F/F_0$. Puffs were applied at 1Hz for 10 times (over 10 s), as indicated by red-shaded boxes. N = 6 flies. **g.** $\Delta F/F_0$ averaged over 10s of puff application. When multiple neurons were recorded from the same fly (max 4 neurons per fly), results were averaged so that each dot represents one fly. N = 6 flies. two-tailed t -test. ** $p < 0.01$. **h.** Time course of the experiment. After 20 min of acclimation, the heartbeat of the fly expressing light-gated cation channel CsChrimson in DA-WED neurons, with ("Ret +") or without ("Ret -") being fed with the co-factor all-trans retinal (ATR) for 2 days prior to experiment, was recorded for 10s, followed by 1s of light application, and 20s of recording. **i.** Time course of the HR (% change from baseline defined as the average during the 10 s preceding puff onset). Red light was shined during the red-shaded time window. Lines and shaded areas represent means and SEM, respectively. N = 19, 22, for Ret-, Ret+, respectively. **j.** Change in HR, calculated for each fly as the % difference between the mean HR during the 1 s following stimulation onset and the mean HR during the 10 s baseline period preceding stimulation. N = 13, 12, for Ret-, Ret+, respectively. * $p < 0.05$, two-tailed t -test. **k.** Model.

To test if increased activities of DA-WED neurons can replace the air puff to induce cardiac deceleration, we photoactivated DA-WED neurons without puff application (Fig. 4h [↗](#)). For this, we expressed a light-gated cation channel CsChrimson in DA-WED neurons, and shined light on the fly's head to activate these neurons. We found that the photoactivation of DA-WED neurons could induce cardiac deceleration by ~10% in the retinal-fed test flies, but not in the retinal-unfed control flies (Fig. 4i, j [↗](#); Supplementary Movie 3 [↗](#)).

Together, our data establishes that DA-WED neurons are responsible for puff-induced cardiac deceleration (Fig. 4k [↗](#)).

V. Cardiac interoception possibly contributes to threat-induced locomotion

Cardiac interoception has recently been implicated in modulating behavioral responses ^{41–43}. We therefore asked whether cardiac deceleration is associated with changes in locomotion in *Drosophila*. To test this, we silenced DA-WED neurons using Kir2.1 to block puff-induced cardiac deceleration, and assessed locomotor output. We found that silencing DA-WED neurons markedly suppressed puff-induced locomotion compared to controls (Fig. 5a, b [↗](#)). Conversely, photoactivation of DA-WED neurons using CsChrimson promoted locomotion in the absence of puff (Fig. 5c, d [↗](#)). These findings suggest that DA-WED neurons coordinate cardiac deceleration with locomotor responses during threat.

An alternative interpretation is that DA-WED neurons function as general threat detectors that broadly regulate puff-evoked behaviors. If this were the case, manipulating these neurons should affect all of behavioral outputs induced by puff. In addition to promoting locomotion, air puff suppressed grooming (Supplementary Fig. 9a, b [↗](#)). However, silencing DA-WED neurons failed to disrupt puff-induced grooming suppression (Supplementary Fig. 9c, d [↗](#)), despite markedly reducing cardiac deceleration (Fig. 4b, c [↗](#)) and locomotion (Fig. 5a, b [↗](#)). Likewise, photoactivation of DA-WED neurons failed to suppress grooming (Supplementary Fig. 9e, f [↗](#)), while robustly inducing cardiac deceleration (Fig. 4b, c [↗](#)) and locomotion (Fig. 5c, d [↗](#)). Thus, manipulation of DA-WED neurons does not reproduce the full behavioral repertoire triggered by puff. These findings argue against the idea that DA-WED neurons function as general threat detectors and instead support a more specific role in coordinating cardiac and locomotor responses.

To directly test whether cardiac deceleration can influence locomotion, we optogenetically mimicked puff-induced cardiac deceleration by expressing the light-gated anion channel GtACR1 in cardiomyocytes using Hand-GAL4 (Fig. 5e [↗](#)). We selected an anion channel to prolong diastole, unlike a previous report using a cation channel⁷⁷, as puff-induced cardiac deceleration is characterized by elongated diastolic intervals (Fig. 1c [↗](#)). Brief green light pulses (28 ms; Fig. 5f [↗](#)) transiently arrested the heart in diastole (Fig. 5g [↗](#); Supplementary Movie 5 [↗](#)), reducing heart rate by ~10% (Fig. 5h, i [↗](#)), comparable to puff- and DA-WED-induced deceleration (Fig. 1d, e [↗](#); Fig. 4i, j [↗](#)). Notably, optogenetic induction of cardiac deceleration in cardiomyocytes— independent of central dopaminergic activation—was accompanied by increased locomotion (Fig. 5j, k [↗](#)). In contrast, this manipulation failed to alter grooming behavior (Supplementary Fig. 9g–i [↗](#)). These observations are consistent with the possibility that cardiac deceleration may influence locomotor responses during threat.

Together, these findings identify DA-WED neurons that drive cardiac deceleration during threat and suggest that the resulting cardiac state may influence locomotor responses (Fig. 5l [↗](#)).

Altogether, these results identify a group of dopaminergic neurons that mediate threat-induced cardiac deceleration and point to a potential role of cardiac dynamics in shaping locomotor responses during threat.

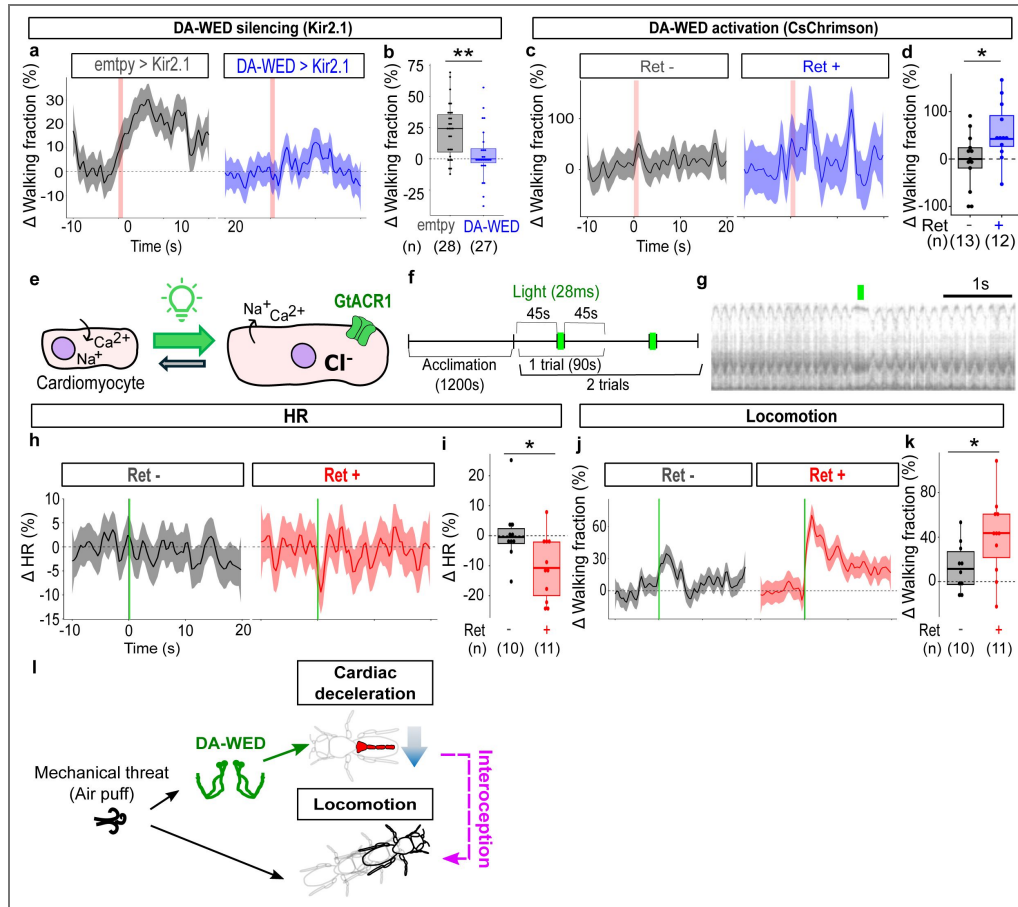


Fig. 5. Cardiac interoception possibly contributes to threat-induced locomotion

a. Time course of the walking fraction (% change from baseline defined as the mean fraction during the 10 s preceding puff onset). An air puff was applied during the red-shaded time window. Lines and shaded areas represent means and SEM, respectively. N = 28, 27, for empty>Kir2.1, DA-WED>Kir2.1, respectively. **b.** Change in walking fraction, calculated for each fly as the % difference between the mean fraction during the 10 s following stimulation onset and the mean fraction during the 10 s baseline period preceding stimulation. N = 28, 27, for empty>Kir2.1, DA-WED>Kir2.1, respectively. ** $p < 0.01$, Two-tailed t -test. **c.** Time course of the walking fraction (% change from baseline defined as the mean fraction during the 10 s preceding puff onset). Red light was applied during the red-shaded time window. Lines and shaded areas represent means and SEM, respectively. N = 13, 12, for ret⁻, +, respectively. **d.** Change in walking fraction, calculated for each fly as the % difference between the mean fraction during the 10 s following stimulation onset and the mean fraction during the 10 s baseline period preceding stimulation. N = 13, 12, for ret⁻, +, respectively. ** $p < 0.01$, Two-tailed t -test. **e.** A schematic of the strategy. Cardiomyocytes beat by oscillating between shrunk (systole) and relaxed (diastole) states. Diastole is driven by efflux of cation and resultant hyperpolarization. We expressed a light-gated anion channel GtACR1 in cardiomyocytes using Hand-GAL4, thus artificially driving hyperpolarization by shining light. **f.** Time course of the experiment. After 20 min of acclimation, the heartbeat of the fly expressing GtACR1 in cardiomyocytes, with or without being fed with the co-factor all-trans retinal (ATR) for 2 days prior to experiment, was recorded for 90s, followed by a 28ms light pulse, and 45s of recording. The experiment was repeated twice for each fly. **g.** An example M-mode during optogenetic cardiac deceleration. Green bar indicates when the light was shined. **h.** Time course of the HR (% change from baseline defined as the average during the 10 s preceding puff onset). Green light was shined during the green-shaded time window. Lines and shaded areas represent means and SEM, respectively. N = 10, 11, for ret⁻, ret⁺, respectively. **i.** Change in HR, calculated for each fly as the % difference between the mean HR during the 1 s following stimulation onset and the mean HR during the 10 s baseline period preceding stimulation. N = 10, 11, for ret⁻, ret⁺, respectively. * $p < 0.05$, Two-tailed t -test. **j.** Time course of the walking fraction (% change from baseline defined as the mean fraction during the 10 s preceding puff onset). Light was shined during the green-shaded time window. Lines and shaded areas represent means and SEM, respectively. N = 10, 11, for ret⁻, ret⁺, respectively. **k.** Change in walking fraction, calculated for each fly as the % difference between the mean fraction during the 10 s following stimulation onset and the mean fraction during the 10 s baseline period preceding stimulation. N = 10, 11, for ret⁻, ret⁺, respectively. * $p < 0.05$, two-tailed t -test. **l.** Model.

Discussion

Here we demonstrate that mechanical threat engages dopaminergic neurons that induce rapid cardiac deceleration and is associated with increased locomotion. Air puff stimulation elicited both cardiac deceleration and locomotor activation (Fig. 1 [↗](#)), and we identified two pairs of dopaminergic neurons, termed DA-WED neurons, as key mediators of the cardiac response (Fig. 4 [↗](#)). Silencing these neurons attenuated threat-induced cardiac deceleration and locomotion, whereas optogenetic activation of DA-WED neurons elicited both responses in the absence of threat (Fig. 4 [↗](#), Fig. 5 [↗](#)). Moreover, direct optogenetic cardiac deceleration was accompanied by increased locomotion (Fig. 5 [↗](#)), suggesting that cardiac deceleration may influence behavioral responses. Together, these findings support a model in which descending dopaminergic control of cardiac activity contributes to the coordination of physiological and behavioral responses to threat, potentially via interoceptive feedback from the heart.

Cardiac deceleration accompanies active defensive locomotion

Our data show that air puff stimulation induces cardiac deceleration together with increased locomotion (Fig. 1 [↗](#)). Stronger puff results in more pronounced locomotion but diminished cardiac deceleration (Fig. 1d-g [↗](#)), suggesting that cardiac deceleration is likely not simply a byproduct of locomotion.

Although cardiac deceleration is often associated with freezing in mammals¹, cardiac deceleration has also been observed during early threat detection and orienting responses⁷⁸, suggesting that it reflects engagement of a defensive processing rather than motor inhibition *per se*. Consistent with this view, dissociation between threat-evoked cardiac modulation and freezing has been reported across taxa. In mammals, for example, disruption of autonomic output can abolish cardiac deceleration without eliminating freezing⁷⁹, suggesting that cardiac deceleration is not merely a secondary consequence of freezing. Similarly, in decapod crustaceans and *Drosophila*, visual stimuli elicit reproducible and time-locked changes in heart rate that accompany both freezing and fleeing^{8,9,80}. Our findings extend these observations by showing that cardiac deceleration can accompany active fleeing behavior in response to mechanical threat. Thus, cardiac deceleration is not restricted to passive defensive strategies but can occur during active locomotor responses, supporting the idea that cardiac dynamics are flexibly coupled to different components of the defensive repertoire.

Dopaminergic neurons in the brain are responsible for puff-induced cardiac deceleration

The present study identifies two pairs of dopaminergic neurons in the brain, termed DA-WED neurons, as key mediators of puff-induced cardiac deceleration. Silencing/ photoactivating DA-WED neurons disrupts/ mimics puff-induced cardiac deceleration, respectively (Fig. 4b, c, h-j [↗](#)). Furthermore, DA-WED neurons exhibit calcium elevation upon air puffs (Fig. 4d-g [↗](#)). Moreover, knockdown of the dopamine synthetic enzyme *ple* in DA-WED neurons suppresses puff-induced cardiac deceleration (Supplementary Fig. 6f-h [↗](#)), suggesting that dopamine release from these neurons is required for cardiac deceleration.

Circulatory dopamine has long been associated with cardiac acceleration across species⁸¹. In *Drosophila*, pharmacological application of DA to the exposed heart accelerates the heartbeat^{60–63}, seemingly at odds with our findings. However, the responsible source of circulatory DA or DA receptor, as well as whether DA directly acts on cardiomyocytes or instead through some yet unidentified cells, remain elusive. In mammals, cardiomyocytes *per se* synthesize DA and express DA receptors, hinting at autocrine mechanism⁸¹. Circulatory DA also increases the levels of epinephrine and norepinephrine, complicating the interpretation of “DA-induced” cardiac acceleration⁸². From our ple RNAi experiment (Supplementary Fig. 6f-h [↗](#)), DA released from DA-WED neurons appears indispensable for puff-induced cardiac deceleration. Notably, neurites of DA-WED neurons never exit the brain, suggesting that DA-WED neurons engage circulation or yet unidentified neuronal circuitry to indirectly modulate the heartbeat.

Circulation is unlikely to mediate DA-WED neurons’ function, however, given that the air puff and DA-WED activation both induce cardiac deceleration within a second (Fig. 1 [↗](#), Fig. 4 [↗](#)). Interestingly, DA acting as a local neuromodulator to drive cardiac deceleration has been documented in mammals by a few literatures, either in the ventral tegmental area (VTA) or lateral habenula (LHb)^{83,84}. Together, our findings and previous literature suggest that dopamine may act not only as a circulating hormone that accelerates heart rate, but as a centrally deployed neuromodulator capable of driving cardiac deceleration during defensive states.

DA-WED neurons coordinate cardiac and behavioral threat responses

Across species, threatening stimulation elicits cardiac and behavioral responses in an orchestrated fashion. Cardiac interoception is postulated to serve as key feedback to link cardiac and behavioral responses³⁹. Cardiac interoception is mediated by sensory neurons innervating the heart and aortic arch³⁹, which convey information to ACC, insular, and prefrontal cortex⁴⁰ through brain stem NTS and hypothalamic PVN⁴⁰. These ascending pathways have been proposed to modulate learned fear⁴¹, anxiety-like behavior⁴² or sleep⁴³. Although models propose that descending control of the heart and ascending interoceptive feedback jointly shape defensive behavior, experimental validation of this bidirectional framework within a single system has been limited.

Our results provide partial support for such a model. We show that (1) mechanical threat induces cardiac deceleration and locomotion (Fig. 1 [↗](#)), (2) DA-WED neurons in the brain are responsible for threat-induced cardiac deceleration (Fig. 4 [↗](#)), (3) optogenetic cardiac deceleration is accompanied by increased locomotion (Fig. 5d-j [↗](#)). Our data points to a scenario in which DA-WED neurons induce cardiac deceleration upon threat, which may in turn influence threat-induced locomotion (Fig. 5k [↗](#)).

Notably, the behavioral consequences of cardiac deceleration appear to be selective rather than global. Although air puff stimulation suppressed grooming, neither silencing nor activation of DA-WED neurons significantly affected grooming responses (Supplementary Fig. 9 [↗](#)), despite robust effects on cardiac deceleration and locomotion (Fig. 4 [↗](#), Fig. 5 [↗](#)). Similarly, direct optogenetic induction of cardiac deceleration failed to influence grooming behavior. These dissociations indicate that cardiac feedback does not uniformly modulate defensive behaviors but preferentially facilitates locomotor output. Such selectivity is consistent with the possibility that interoceptive signals from the heart may bias specific behavioral strategies rather than simply increasing overall arousal.

Our data suggest that descending dopaminergic control of cardiac function and ascending cardiac feedback may form a functional loop that shapes adaptive defensive behavior. Although the specific cardiac sensory pathways mediating feedback to the brain remain to be identified in *Drosophila*, future work may determine whether flies possess interoceptive circuits functionally analogous to vertebrate NTS–PVN pathways. Establishing such circuitry would provide a powerful platform to dissect how central commands and peripheral physiological states interact to coordinate survival behaviors.

Limitations of this study

While our data are consistent with a model in which DA-WED neurons couple cardiac deceleration to locomotor responses during threat, several questions remain.

Although cardiac deceleration can promote locomotion, we have not directly tested whether it is required for DA-WED-evoked locomotion, leaving open the possibility of parallel downstream pathways. In addition, the sensory mechanisms that relay cardiac state to locomotor circuits in *Drosophila* remain unidentified. Finally, despite the rapid timescale and behavioral specificity of our manipulations, we cannot fully exclude indirect physiological contributions secondary to altered cardiac dynamics. Future dissection of descending and ascending circuits will clarify these mechanisms.

Overall, we identify a discrete population of dopaminergic neurons that drive rapid cardiac deceleration in response to mechanical threat. We further show that these neurons coordinate cardiac responses and are associated with behavioral components of the defensive response, potentially by engaging interoceptive feedback from the heart. Our findings establish *Drosophila* as a tractable model for dissecting how exteroceptive and interoceptive signals are integrated to couple organ physiology with adaptive behavior, opening new avenues for understanding the neural logic by which internal and external states are coordinated to promote survival.

Methods

Fly stocks

The following strains were obtained from Bloomington Stock Center (Indiana University): TrH-GAL4 (#38388), Tdc2-GAL4 (#9313), TH-GAL4 (#8848), UAS-TNT (#28838), UAS-Kir2.1::EGFP (#6596), UAS-CsChrimson::mVenus (#55135), UAS-dTrpA1 (#26263), UAS-mCD8::GFP (#32186), UAS-RedStinger (#8547), UAS-IVS-jGCaMP7s (#79032), UAS-GFP RNAi (#41560), UAS-Ple RNAi (#65875), VT046828-AD (#73115), R12D12-DBD (#69213), R48A08-AD (#70707), VT008692-DBD (#86909), empty-AD; empty-DBD (#79603), R70G12-GAL4 (#39552), R38B08-AD (#71032), R81E10-DBD (#68529), VT043775-DBD (#73728), R74C07-GAL4 (#39847), Aes1N-GAL4 (#39847), iav-GAL4 (#52273), R48A07-GAL4 (#50340), UAS-mCherry (#52267), Hand-GAL4 (#48396).

The following strains were obtained from Kyoto *Drosophila* Stock Center (Kyoto Institute of Technology): Tes1N-GAL4 (#103660).

Hand-GFP was a gift from Dr. Zhe Han (The University of Maryland).

UAS-FRT-stop-FRT-Kir2.1, and UAS-FRT-stop-FRT-CsChrimson::mVenus were gifts from Dr. Barry Dickson (The University of Queensland).

TH-C-GAL4, TH-D-GAL4, TH-F1-GAL4, Vmat-R76F01-GAL4, Vmat-R76F05-GAL4, Ddc-R61H03-GAL4, Ddc-R60F07-GAL4, DAT-R55C10-GAL4, Vmat-R76F01-AD, Vmat-R76F05-AD, Ddc-R60F07-AD, Vmat-R76F01-DBD, Vmat-R76F05-DBD, Ddc-R60F07-DBD, TH-FLP, UAS-FsF-mCD8GFP were gifts from Dr. Mark Wu (Johns Hopkins University).

Dop1R1-attP, *Dop1R2-attP*, *Dop2R-attP*, *DopEcR-attP*, *TrH-attP* were gifts from Dr. Yi Rao (Peking University).

UAS-GtACR1::tdTomato (III) was gift from Dr. Tabata (The University of Tokyo).

Genotypes and sample sizes used in this study are summarized in [Supplementary Data 1](#).

Fly husbandry

Flies were maintained on conventional cornmeal-agar-molasses medium under a 9AM:9PM light/dark cycle at 25 °C and 60 +/- 5 % humidity. Flies were collected 0–1 day post eclosion and housed in a group of 9–10 for 2–5 days before testing unless otherwise stated. Male flies were used throughout except for [Supplementary Fig. 4h, i](#), in which both male and female were used. All experiments were carried out between 10 am and 8 pm at 25 +/- 0.8 C and 60 +/- 5 % humidity.

Heartbeat and behavior recording

Flies were tethered above an air-supported foam ball (8 mm diameter; Yuzawaya, Japan) mounted in a custom sphere holder. Airflow was continuously monitored using a digital flowmeter (MF-FP10N-H06-010, Horiba Estec Inc.) and maintained at 500 ± 10 mL/min. Behavioral imaging was performed from the right side under 850 nm infrared illumination using a CMOS camera (GE60, Himawari; 640×480 pixels).

Simultaneously, cardiac activity was imaged from the dorsal side through the intact cuticle under 850 nm illumination using a second CMOS camera (CS135MU, Thorlabs; 800×500 pixels). Behavioral and cardiac imaging streams were externally triggered and synchronized at 70 Hz using an Arduino Uno board.

Immediately prior to the experiment, flies were briefly (< 1 min) cold-anesthetized, and the dorsal thorax and abdomen were glued to a coverslip using UV-curable adhesive (Bondic BD-SKCJ) polymerized with 405 nm UV light (OSV5XME1C1E, Akizuki Electronics Inc.). The coverslip was positioned above the air-supported ball, allowing the fly to freely walk on the ball. Each recording session, except for DA-WED optogenetic activation experiment, consisted of a 20 min acclimation period followed by puff-response testing (950 s). During puff-response testing, a 500 ms air puff was delivered once every 90 s for a total of 10 puffs. Recording continued for 30 s after the final puff. DA-WED optogenetic activation experiment consisted of a 20 min acclimation period followed by photoactivation-response testing (950 s), in which a 1 s 617nm light was delivered once every 90 s for a total of two (See “Optogenetic activation of DA-WED neurons” below), to avoid potential desensitization of CsChrimson.

Heartbeat (without behavior) recording

Cardiomyocytes expressing GFP were imaged dorsally through the intact cuticle. Images (104×50 pixels) were acquired at 24 Hz using a Leica SP8 confocal microscope equipped with a $10\times$ objective lens (NA 0.4).

Immediately before recording, flies were briefly (< 1 min) cold-anesthetized, and the ventral thorax and abdomen were glued to a glass slide using UV-curable adhesive (Bondic BD-SKCJ) polymerized with 405 nm UV light (OSV5XME1C1E, Akizuki Electronics Inc.). The slide was positioned beneath the objective lens for imaging. Each recording session consisted of a 10 min acclimation period followed by puff-response testing (350 s total). A single puff-response test consisted of 1 min baseline recording, followed by a train of 10 air puffs delivered at 1 Hz (10 s total), and a subsequent 1 min post-stimulation recording. For each fly, the puff-response test was repeated twice with a 90 s inter-trial interval.

Automatic heartbeat detection

To automatically detect individual heartbeats, we developed custom software tools. For infrared (IR)-based heart imaging obtained during simultaneous recordings of cardiac activity and behavior, the detection pipeline (Supplementary Fig. 1a [↗](#)) computed optical flow for each pixel between consecutive video frames. These optical flow measurements were used to quantify global cardiac relaxation (diastole) and contraction (systole). Time points corresponding to maximal contraction were identified as systolic peaks, and peak counts were used to compute heart rate (HR). The precision of the automated detection was evaluated by comparing both absolute HR values and percent changes in HR during air-puff stimulation relative to baseline with manual annotations. These analyses demonstrated that the automated method detected both absolute HR and stimulus-evoked HR changes with accuracy indistinguishable from manual scoring (Supplementary Fig. 1b, c [↗](#)).

To detect heartbeats in confocal microscopy images of GFP-expressing cardiomyocytes (recorded in the absence of behavioral measurements; Supplementary Fig. 4a [↗](#)), each frame was subtracted from the subsequent frame to compute pixel-wise differences between consecutive image pairs. This procedure generated positive and negative pixel values in regions surrounding the cardiomyocytes during cardiac contraction (systole) and relaxation (diastole). During systole,

pixels within the heart tube exhibited positive values corresponding to the current positions of cardiomyocytes, whereas pixels outside the heart tube exhibited negative values corresponding to their previous positions; the opposite pattern was observed during diastole. Systolic and diastolic phases were distinguished by: (i) calculating the standard deviation of the positions of positive-value pixels along the axis perpendicular to the heart tube (the y-axis in [Supplementary Fig. 4a](#)), denoted $SD(t)$; (ii) calculating the standard deviation of the positions of negative-value pixels along the same axis, denoted $SD(t-1)$; and (iii) computing the difference $SD(t) - SD(t-1)$. Negative values of $SD(t) - SD(t-1)$ indicated systole, whereas positive values indicated diastole ([Supplementary Fig. 4a](#)). Time points corresponding to maximal contraction were identified as systolic peaks, and peak counts were used to compute HR. The precision of this algorithm was evaluated as described above. Although absolute HR values were slightly overestimated ([Supplementary Fig. 4b](#)), stimulus-evoked changes in HR were captured with accuracy indistinguishable from manual annotation ([Supplementary Fig. 4c](#)).

To obtain a continuous HR time course, peak counts were binned into 0.2 s intervals, and the number of beats per bin was calculated for each fly and trial. For visualization of HR dynamics relative to stimulus onset, HR traces were aligned to puff onset (time 0) and averaged across repeated trials within each fly. In experiments with a single air puff, puff-induced HR modulation was quantified by comparing the mean HR during the 1 s following puff onset with the mean HR during the 10 s baseline period preceding puff onset. Percent change was calculated as $[(HR_{post} - HR_{baseline}) / HR_{baseline}] \times 100$. In experiments involving 10 puffs delivered over a 10 s window, HR modulation was quantified as the mean HR during the entire 10 s stimulation period relative to the 10 s pre-stimulus baseline.

Automatic behavioral identification

To automatically identify behavior on a frame-by-frame basis, videos were analyzed offline using a custom Python-based pipeline. Body-part coordinates—including the joints of each leg, the eye, neck, haltere, and the rostral tip of the abdomen on the right side of the fly—were tracked using SLEAP software⁵⁴. The tracked coordinates were subsequently transformed to normalize body length and orientation across individuals. Using these standardized coordinates, the speed of each body part was calculated for each pair of consecutive frames. Both the standardized coordinates and corresponding speed measurements were then provided as inputs to a custom support vector machine (SVM)-based classifier, which labeled each frame as “groom,” “walk,” or “halt.” The SVM was trained using the standardized body-part coordinates and speed features as predictors, with manually annotated behavioral labels serving as the dependent variables. For each fly and each time point relative to puff onset, we calculated the fraction of frames classified as walking or grooming across 10 repeated trials. For visualization of behavioral dynamics, these fraction time courses were aligned to puff onset (time 0) and averaged across trials within each fly. Puff-induced changes in walking and grooming were quantified by comparing the mean fraction during the 10 s and 3 s, respectively, following puff onset with the mean fraction during the 10 s baseline period preceding puff onset. Percent change was calculated as $[(fraction_{post} - fraction_{baseline}) / fraction_{baseline}] \times 100$.

Mechanical stimulation

Mechanical stimulation was delivered through a glass pipette (tip diameter of ~2 mm), placed ~2mm in front of the fly, connected with air hose to a compressor (EARTH MAN, Takagi, Japan) via a solenoid valve (EXA-C6-02C-4, CKD). The solenoid valve was controlled by an Arduino Uno board, which in turn received connection from a desktop computer running the python program which orchestrated the video recordings and puff application. The mechanical stimulation was generated by alternating the solenoid valve between 500 ms-open and 500 ms-closed states (1 Hz). The mechanical stimulation lasted for either 1s, 10s, or 20s, as specified in each figure. The air flow was monitored with a digital flowmeter (MF-FP10N-H06-010, Horiba estec. Inc) and was adjusted to either 20 mL, 50 mL, or 200 mL/min, as specified in each figure.

Optogenetic activation of DA-WED neurons

Flies expressing CsChrimson, a red-shifted channelrhodopsin variant, in DA-WED neurons were raised on food containing 500 μM all-trans retinal for 2 - 3 days, in the dark, prior to testing. Photoactivation was performed by delivering a 1s LED light pulse (617nm, Thorlabs) to the fly's head. The output for LED was measured with a power meter (S120C and PM120D, Thorlabs) at a position corresponding to the fly's head, and was adjusted to 1 $\mu\text{W}/\text{mm}^2$. Light stimuli were triggered by python through an Arduino board connected to the LED driver.

Optogenetic cardiac deceleration

Flies expressing GtACR1, a light-gated anion channel, in cardiomyocytes were raised on food containing 500 μM all-trans retinal for 2 - 3 days, in the dark, prior to testing. Photoactivation was performed by delivering a 28ms-long LED light pulse (530nm, Thorlabs) to the fly's heart through the objective lens. The light intensity was adjusted, for each fly prior to the recording, to the minimum intensity required for a light pulse of roughly 2s to briefly stop the heartbeat. After the recording, the output for LED was measured with a power meter (S120C and PM120D, Thorlabs) at a position corresponding to the fly's heart, and ranged from 9.88 – 21.8 $\mu\text{W}/\text{mm}^2$. Light stimuli were triggered by python through an Arduino board connected to the LED driver.

Immunohistochemistry

The following antibodies were used: mouse nc82 (1:10 Developmental Studies Hybridoma Bank), goat anti-mouse Alexa 633 (1:100, Molecular Probe #A21050). Whole brain immunohistochemistry was performed as described previously^{85,86}. Briefly, brains were dissected out in 0.3 % PBST, and were fixed in 2 % paraformaldehyde/ PBS for 90 min at room temperature. Brains were then washed in 0.3 % PBST, for > 3 h, and were blocked in 10 % normal goat serum/ 0.3 % PBST for 30 min. Brains were incubated in the primary antibodies in 10% normal goat serum/ 0.3% PBST at 4 °C for 2 days. Brains were then washed in 0.3 % PBST for > 5 h, and were blocked in 10 % normal goat serum/ 0.3 % PBST for 30 min. Brains were then incubated in the secondary antibodies in 10 % normal goat serum/ 0.3 % PBST at 4°C for 2 days. Afterward, brains were washed in 0.3 % PBST for > 5 h, and incubated in 50 % glycerol/ 0.3 % PBST for 2 h at 4 °C. Lastly, brains were mounted on slide glass in Vectashield (Vector Laboratories). Images were taken with Leica TCS SP8 confocal microscope, and processed in ImageJ (NIH) software.

Calcium imaging

Two-photon calcium imaging was conducted as described previously⁵³ with a few modifications. Two-photon microscopy (Bergamo II, Thorlabs) with a 16x objective lens (16x CFI LWP Plan Flour Objective, Nikon) and with near-infrared excitation (930 nm, Mai Tai 2, SpectraPhysics, Inc., Mountain View, CA) was used. Cuticle of the top of the flies' head and the fat and trachea beneath it were surgically removed. The exposed brain was submerged in saline solution. The extracellular saline had the following composition (in mM): 103 NaCl, 3 KCl, 5 HEPES, 10 trehalose, 10 glucose, 7 sucrose, 26 NaHCO_3 , 1 NaH_2PO_4 , 1.5 CaCl_2 , 4 MgCl_2 . We identified DA-WED neurons using the baseline fluorescence of GCaMP. Images were acquired from 1 plane at 152 frames per s (160 x 96 pixels, pixel size = 0.388 μm , dwell time = 0.246 μs). During calcium imaging, a large fraction of the fly's body was glued to the holding plate, and part of the fly's eye compounds was covered with the holder, and the fly was hung in the air. Each fly underwent the sequence of stimuli per fly once or twice, to scan DA-WED neurons on both hemispheres whenever possible. The time courses of $\Delta F/F_0$ were calculated by, for each bin, taking the percent difference from F_0 10s prior to the onset of the initial puff application ($t = -10$ through 0s in Fig. 4f³).

Surgery

In search of sensory organs indispensable for air puffs to induce cardiac deceleration, halteres, wings, legs, and a3 segments of the antennae were surgically removed using a pair of forceps on ice just prior to testing. Flies that underwent cold anesthesia just prior to testing served as

controls.

Feeding preference test

Two days post eclosion male flies were protein deprived by maintaining on 200 mM sucrose (vials with a kimwipe soaked with 2mL of sucrose solution) for 8 days (kimwipe is exchanged every other day). Prep 7.5% yeast and 200mM sucrose in 0.9% of agar, color-labeled with either blue (brilliant blue FCF) or red (sulforhodamine B) tasteless food dyes. The two types of food mix, 1mL each, were then aliquoted into 35mm petri dish separated by a 5×5×35mm acrylic bar into two chambers. A group of 70 flies starved for 3 hours in an empty vial with a kimwipe soaked with 2 mL of water were cold-anesthetized and transferred into petri dish at ZT2 and allowed to feed for 2 hours in the dark. The flies were then killed by transferring the dish to -30C, upside-down, and scored by examining the color of their abdomen. Preference Index (PI) for yeast was calculated as (# flies consuming yeast - # flies consuming sucrose) / (total # flies that fed). Flies with insufficiently colored abdomen were discarded as poorly fed flies.

Data analyses

Data analyses were performed using our custom-written R and python programs.

Statistics

We did not predetermine the sample sizes. The distribution of normality of each group was assessed using Shapiro-Wilk normality test. Parametric tests (unequal variances *t*-test known as Welch's *t*-test or Dunnett's test) were used only when distributions were deemed normal; otherwise, non-parametric tests were used (Wilcoxon signed rank test, Wilcoxon rank sum test, or Dunn's test). All statistical tests were two-sided. We employed Bonferroni correction to correct for two tests, and correction implemented in Dunnett's or Dunn's test for more than two tests. $p < 0.05$ after corrections for multiple comparison was deemed statistically significant. Neither randomization nor blinding was performed for the group allocation during experiments or data analysis. All box plots are generated so that center line indicates median, box limits indicate upper and lower quartiles, and whiskers indicate 1.5x interquartile range. All the statistical results are summarized in [Supplementary Data 2](#).

Data availability

All data used to generate the figures are available in [Source Data](#). Source codes used in the current study are available at https://github.com/mtsuj172/heart_behavior.

Acknowledgements

We thank T. Katsuki (ThorLabs) for technical support in setting up the hardware; members of the Emoto Lab for advice and support. This study was supported by JSPS (KAKENHI 24K18157), JST (ACT-X JPMJAX242D), Yamaguchi Educational and Scholarship Foundation to M.T., AMED-CREST (JP21gm310010), Takeda Science Foundation, Torray Foundation, Naito Foundation, and WPI-IRC to K.E.

Additional information

Author contributions

M.T. designed the experiments. M.T., J. D., Y. U., and A.O. performed the experiments. M.T. analyzed the data. M.T. and K.E. interpreted the results and wrote the paper.

Funding

Funder	Grant reference number	Author
MEXT Japan Society for the Promotion of Science (JSPS)	KAKENHI 24K18157	Masato Tsuji
MEXT Japan Science and Technology Agency (JST)	https://doi.org/10.52926/jpmjax242d	Masato Tsuji
Yamaguchi Educational and Scholarship Foundation		Masato Tsuji
Japan Agency for Medical Research and Development (AMED)	JP21gm310010	Kazuo Emoto
Takeda Science Foundation (TSF)		Kazuo Emoto
Torray Foundation		Kazuo Emoto
Naito Foundation (内藤記念科学振興財団)		Kazuo Emoto
WPI-IRCN		Kazuo Emoto

Author ORCID iDs

Masato Tsuji:  <https://orcid.org/0000-0001-8181-7968>

Kazuo Emoto:  <https://orcid.org/0000-0003-4194-801X>

Additional files

[Supplementary Figures](#) 

[Supplementary Movie 1](#) 

[Supplementary Movie 2](#) 

[Supplementary Movie 3](#) 

[Supplementary Movie 4](#) 

[Supplementary Movie 5](#) 

[Supplementary Data 1](#) 

[Supplementary Data 2](#) 

[Source Data](#) 

References

1. Hagenaaers M. A., Oitzl M., Roelofs K. (2014) Updating freeze: Aligning animal and human research. *Neuroscience and Biobehavioral Reviews* **47**:165-176 <https://doi.org/10.1016/j.neubiorev.2014.07.021> | PubMed
2. Babo-Rebello M., Richter C. G., Tallon-Baudry C (2016) Neural Responses to Heartbeats in the Default Network Encode the Self in Spontaneous Thoughts. *Journal of Neuroscience* **36**:7829-7840 <https://doi.org/10.1523/jneurosci.0262-16.2016> | PubMed
3. Jammal Salameh L., Bitzenhofer S. H., Hanganu-Opatz I. L., Dutschmann M., Egger V. (2024) Blood pressure pulsations modulate central neuronal activity via mechanosensitive ion channels. *Science* **383**:eadk8511 <https://doi.org/10.1126/science.adk8511> | PubMed
4. Azzalini D., Buot A., Palminteri S., Tallon-Baudry C (2021) Responses to heartbeats in ventromedial prefrontal cortex contribute to subjective preference-based decisions. *The Journal of Neuroscience* **41** <https://doi.org/10.1523/jneurosci.1932-20.2021> | PubMed
5. Ran C., Boettcher J. C., Kaye J. A., Gallori C. E., Liberles S. D (2022) A brainstem map for visceral sensations. *Nature* **609** <https://doi.org/10.1038/s41586-022-05139-5> | PubMed

6. Lang P. J., Davis M., Öhman A (2000) Fear and anxiety: Animal models and human cognitive psychophysiology. *J. Affect. Disord* **61**:137-159 [https://doi.org/10.1016/s0165-0327\(00\)00343-8](https://doi.org/10.1016/s0165-0327(00)00343-8) | PubMed
7. Gordan R., Gwathmey J. K., Xie L.-H (2015) Autonomic and endocrine control of cardiovascular function. *World J. Cardiol* **7**:204 <https://doi.org/10.4330/wjc.v7.i4.204> | PubMed
8. Pérez-Schuster V., et al. (2024) Threatening stimuli elicit a sequential cardiac pattern in arthropods. *iScience* **27**:108672 <https://doi.org/10.1016/j.isci.2023.108672> | PubMed
9. Burnovicz A., Oliva D., Hermitte G (2009) The cardiac response of the crab *Chasmagnathus granulatus* as an index of sensory perception. *Journal of Experimental Biology* **212**:313-324 <https://doi.org/10.1242/jeb.022459> | PubMed
10. Koba S., et al. (2022) A brainstem monosynaptic excitatory pathway that drives locomotor activities and sympathetic cardiovascular responses. *Nature communications* <https://doi.org/10.1038/s41467-022-32823-x> | PubMed
11. Green A. L., et al. (2007) Identifying cardiorespiratory neurocircuitry involved in central command during exercise in humans. *Journal of Physiology* **578**:605-612 <https://doi.org/10.1113/jphysiol.2006.122549> | PubMed
12. Matsukawa K. (2012) Central command: Control of cardiac sympathetic and vagal efferent nerve activity and the arterial baroreflex during spontaneous motor behaviour in animals. *Experimental Physiology* **97**:20-28 <https://doi.org/10.1113/expphysiol.2011.057661> | PubMed
13. Yoshimoto A., Morikawa S., Kato E., Takeuchi H., Ikegaya Y (2024) Top-down brain circuits for operant bradycardia. *Science* **384**:1361-1368 <https://doi.org/10.1126/science.adl3353> | PubMed
14. Wink J., et al. (2020) Human adult cardiac autonomic innervation: Controversies in anatomical knowledge and relevance for cardiac neuromodulation. *Autonomic Neuroscience: Basic and Clinical* **227** <https://doi.org/10.1016/j.autneu.2020.102674> | PubMed
15. White D. W., Raven P. B (2014) Autonomic neural control of heart rate during dynamic exercise: Revisited. *Journal of Physiology* **592**:2491-2500 <https://doi.org/10.1113/jphysiol.2014.271858> | PubMed
16. Rajendran P. S., et al. (2019) Identification of peripheral neural circuits that regulate heart rate using optogenetic and viral vector strategies. *Nat. Commun* **10**:1-13 <https://doi.org/10.1038/s41467-019-09770-1> | PubMed
17. Silvani A., Calandra-Buonaura G., Dampney R. A. L., Cortelli P. (2016) Brain-heart interactions: Physiology and clinical implications. *Philosophical Transactions of the Royal Society A: Mathematical, Physical and Engineering Sciences* **374** <https://doi.org/10.1098/rsta.2015.0181> | PubMed
18. Prescott S. L., Liberles S. D (2022) Internal senses of the vagus nerve. *Neuron* **110**:579-599 <https://doi.org/10.1016/j.neuron.2021.12.020> | PubMed
19. Veerakumar A., Yung A. R., Liu Y., Krasnow M. A (2022) Molecularly defined circuits for cardiovascular and cardiopulmonary control. *Nature* **2022**:1-8 <https://doi.org/10.1038/s41586-022-04760-8> | PubMed
20. Silva B. A., Gross C. T., Gräff J., Gra J (2016) The neural circuits of innate fear : detection, integration, action, and memorization. *Learning and Memory* **23**:544-555 <https://doi.org/10.1101/lm.042812.116> | PubMed
21. Headley D. B., Kanta V., Kyriazi P., Paré D (2019) Embracing Complexity in Defensive Networks. *Neuron* **103**:189-201 <https://doi.org/10.1016/j.neuron.2019.05.024> | PubMed
22. Gross C. T., Canteras N. S (2012) The many paths to fear. *Nat. Rev. Neurosci* **13**:651-658 <https://doi.org/10.1038/nrn3301> | PubMed
23. Kreibitz S. D. (2010) Autonomic nervous system activity in emotion: A review. *Biological Psychology* **84**:394-421 <https://doi.org/10.1016/j.biopsycho.2010.03.010> | PubMed
24. Battaglia S., Thayer J. F (2022) Functional interplay between central and autonomic nervous systems in human fear conditioning. *Trends Neurosci* **0** <https://doi.org/10.1016/j.tins.2022.04.003> | PubMed

25. Casto R., Nguyen T., Printz M. P (1989) Characterization of cardiovascular and behavioral responses to alerting stimuli in rats. *American Journal of Physiology-Regulatory, Integrative and Comparative Physiology* **256**:R1121-R1126 <https://doi.org/10.1152/ajpregu.1989.256.5.r1121> | PubMed
26. Dielenberg R. A., Carrive P., McGregor I. S (2001) The cardiovascular and behavioral response to cat odor in rats: unconditioned and conditioned effects. *Brain Res* **897**:228-237 [https://doi.org/10.1016/s0006-8993\(01\)02227-2](https://doi.org/10.1016/s0006-8993(01)02227-2) | PubMed
27. Signoret-Genest J., et al. (2023) Integrated cardio-behavioral responses to threat define defensive states. *Nat. Neurosci* **26** <https://doi.org/10.1038/s41593-022-01252-w> | PubMed
28. Hashemi M. M., et al. (2019) Neural Dynamics of Shooting Decisions and the Switch from Freeze to Fight. *Sci. Rep* **9** <https://doi.org/10.1038/s41598-019-40917-8> | PubMed
29. Farkas E., Jansen A. S. P., Loewy A. D (1998) Periaqueductal gray matter input to cardiac-related sympathetic premotor neurons. *Brain Res* **792**:179-192 [https://doi.org/10.1016/s0006-8993\(98\)00029-8](https://doi.org/10.1016/s0006-8993(98)00029-8) | PubMed
30. Horiuchi J., McDowall L. M., Dampney R. A. L (2006) Differential control of cardiac and sympathetic vasomotor activity from the dorsomedial hypothalamus. *Clin. Exp. Pharmacol. Physiol* **33**:1265-1268 <https://doi.org/10.1111/j.1440-1681.2006.04522.x> | PubMed
31. Alexander L., et al. (2020) Over-activation of primate subgenual cingulate cortex enhances the cardiovascular, behavioral and neural responses to threat. *Nat. Commun* **11**:1-14 <https://doi.org/10.1038/s41467-020-19167-0> | PubMed
32. Koba S., Inoue R., Watanabe T (2016) Role played by periaqueductal gray neurons in parasympathetically mediated fear bradycardia in conscious rats. *Physiol. Rep* **4**:e12831 <https://doi.org/10.14814/phy2.12831> | PubMed
33. Nakamura K., Nakamura Y., Kataoka N (2021) A hypothalamomedullary network for physiological responses to environmental stresses. *Nature Reviews Neuroscience* **23**:35-52 <https://doi.org/10.1038/s41583-021-00532-x> | PubMed
34. Hermans E. J., Henckens M. J. A. G., Roelofs K., Fernández G (2013) Fear bradycardia and activation of the human periaqueductal grey. *Neuroimage* **66**:278-287 <https://doi.org/10.1016/j.neuroimage.2012.10.063> | PubMed
35. Samuels B. C., Zaretsky D. V., DiMicco J. A (2002) Tachycardia evoked by disinhibition of the dorsomedial hypothalamus in rats is mediated through medullary raphe. *Journal of Physiology* **538**:941-946 <https://doi.org/10.1113/jphysiol.2001.013302> | PubMed
36. Rahmouni K (2016) Cardiovascular Regulation by the Arcuate Nucleus of the Hypothalamus. *Hypertension* **67**:1064-1071 <https://doi.org/10.1161/hypertensionaha.115.06425> | PubMed
37. Li S. J., et al. (1996) Melanocortin antagonists define two distinct pathways of cardiovascular control by α - and γ -melanocyte-stimulating hormones. *Journal of Neuroscience* **16**:5182-5188 <https://doi.org/10.1523/jneurosci.16-16-05182.1996> | PubMed
38. Mastrianni J. A., Palkovits M., Kunos G (1989) Activation of brainstem endorphinergic neurons causes cardiovascular depression and facilitates baroreflex bradycardia. *Neuroscience* **33**:559-566 [https://doi.org/10.1016/0306-4522\(89\)90408-9](https://doi.org/10.1016/0306-4522(89)90408-9) | PubMed
39. Lovelace J. W., Ma J., Augustine V. (2024) II Defining cardioception : Heart-brain crosstalk. *Neuron* 1-4 <https://doi.org/10.1016/j.neuron.2024.10.009> | PubMed
40. Shivkumar K., et al. (2016) Clinical neurocardiology defining the value of neuroscience-based cardiovascular therapeutics. *Journal of Physiology* **594**:3911-3954 <https://doi.org/10.1113/jp271870> | PubMed
41. Klein A. S., Dolensek N., Weiland C., Gogolla N (2021) Fear balance is maintained by bodily feedback to the insular cortex in mice. *Science*. **374**:1010-1015 <https://doi.org/10.1126/science.abj8817> | PubMed
42. Hsueh B., et al. (2023) Cardiogenic control of affective behavioural state. *Nature* <https://doi.org/10.1038/s41586-023-05748-8> | PubMed

43. Yao Y., et al. (2022) Cardiovascular baroreflex circuit moonlights in sleep control. *Neuron* **0** <https://doi.org/10.1016/j.neuron.2022.08.027> | PubMed
44. Han Z., Yi P., Li X., Olson E. N (2006) Hand, an evolutionarily conserved bHLH transcription factor required for Drosophila cardiogenesis and hematopoiesis. *Development* **133**:1175-1182 <https://doi.org/10.1242/dev.02285> | PubMed
45. Han Z., Olson E. N (2005) Hand is a direct target of Tinman and GATA factors during Drosophila cardiogenesis and hematopoiesis. *Development* **132**:3525-3536 <https://doi.org/10.1242/dev.01899> | PubMed
46. Sellin J., Albrecht S., Kölsch V., Paululat A (2006) Dynamics of heart differentiation, visualized utilizing heart enhancer elements of the Drosophila melanogaster bHLH transcription factor Hand. *Gene Expression Patterns* **6**:360-375 <https://doi.org/10.1016/j.modgep.2005.09.012> | PubMed
47. Wessells R. J., Bodmer R (2004) Screening assays for heart function mutants in Drosophila. *Biotechniques* **37**:58-66 <https://doi.org/10.2144/04371st01> | PubMed
48. Hillyer J. F., Pass G (2019) The Insect Circulatory System: Structure, Function, and Evolution. *Annu Rev Entomol* <https://doi.org/10.1146/annurev-ento-011019-025003> | PubMed
49. Rotstein B., Paululat A (2016) On the morphology of the drosophila heart. *Journal of Cardiovascular Development and Disease* **3** <https://doi.org/10.3390/jcdd3020015> | PubMed
50. Dulcis D., Levine R. B (2005) Glutamatergic innervation of the heart initiates retrograde contractions in adult Drosophila melanogaster. *Journal of Neuroscience* **25**:271-280 <https://doi.org/10.1523/jneurosci.2906-04.2005> | PubMed
51. Dulcis D., Levine R. B (2003) Innervation of the heart of the adult fruit fly, Drosophila melanogaster. *Journal of Comparative Neurology* **465**:560-578 <https://doi.org/10.1002/cne.10869> | PubMed
52. Barrios N., Farias M., Moita M. A (2021) Threat induces cardiac and metabolic changes that negatively impact survival in flies. *Current Biology* **0** <https://doi.org/10.1016/j.cub.2021.10.013> | PubMed
53. Tsuji M., Nishizuka Y., Emoto K (2023) Threat gates visual aversion via theta activity in Tachykinergic neurons. *Nat. Commun* **14**:3987 <https://doi.org/10.1038/s41467-023-39667-z> | PubMed
54. Pereira T. D., et al. (2022) SLEAP: A deep learning system for multi-animal pose tracking. *Nature Methods* **19**:486-495 <https://doi.org/10.1038/s41592-022-01426-1> | PubMed
55. Tsubouchi A., et al. (2017) Topological and modality - specific representation of somatosensory information in the fly brain. *Science* **623**:615-623 <https://doi.org/10.1126/science.aan4428> | PubMed
56. Zhang N., Guo L., Simpson J. H (2020) Spatial Comparisons of Mechanosensory Information Govern the Grooming Sequence in Drosophila. *Current Biology* **30**:988-1001.e4 <https://doi.org/10.1016/j.cub.2020.01.045> | PubMed
57. Lebestky T., et al. (2009) Two Different Forms of Arousal in Drosophila Are Oppositely Regulated by the Dopamine D1 Receptor Ortholog DopR via Distinct Neural Circuits. *Neuron* **64**:522-536 <https://doi.org/10.1016/j.neuron.2009.09.031> | PubMed
58. Zhang F., Zhao Y., Han Z (2013) An in vivo functional analysis system for renal gene discovery in Drosophila pericardial nephrocytes. *Journal of the American Society of Nephrology* **24**:191-197 <https://doi.org/10.1681/asn.2012080769> | PubMed
59. Keller N. R., et al. (2004) Norepinephrine transporter-deficient mice exhibit excessive tachycardia and elevated blood pressure with wakefulness and activity. *Circulation* **110**:1191-1196 <https://doi.org/10.1161/01.cir.0000141804.90845.e6> | PubMed
60. Zornik E., Paisley K., Nichols R (1999) Neural transmitters and a peptide modulate Drosophila heart rate. *Peptides* **20**:45-51 [https://doi.org/10.1016/s0196-9781\(98\)00151-x](https://doi.org/10.1016/s0196-9781(98)00151-x) | PubMed
61. Zhu Y. C., Yocom E., Sifers J., Uradu H., Cooper R. L (2016) Modulatory effects on Drosophila larva hearts: room temperature, acute and chronic cold stress. *J. Comp. Physiol. B* **186**:829-41 <https://doi.org/10.1007/s00360-016-0997-x> | PubMed

62. Johnson E., Ringo J., Dowse H (1997) Modulation of drosophila heartbeat by neurotransmitters. *J. Comp. Physiol. B* **167**:89-97 <https://doi.org/10.1007/s003600050051> | PubMed
63. Hillyer J. F. (2018) Insect heart rhythmicity is modulated by evolutionarily conserved neuropeptides and neurotransmitters. *Current Opinion in Insect Science* **29**:41-48 <https://doi.org/10.1016/j.cois.2018.06.002> | PubMed
64. Majeed Z. R., Stacy A., Cooper R. L (2014) Pharmacological and genetic identification of serotonin receptor subtypes on Drosophila larval heart and aorta. *J. Comp. Physiol. B* **184**:205-219 <https://doi.org/10.1007/s00360-013-0795-7> | PubMed
65. Johnson E., Sherry T., Ringo J., Dowse H (2002) Modulation of the cardiac pacemaker of Drosophila: Cellular mechanisms. *J. Comp. Physiol. B* **172**:227-236 <https://doi.org/10.1007/s00360-001-0246-8> | PubMed
66. Schroeder C., Jordan J (2012) Norepinephrine transporter function and human cardiovascular disease. *American Journal of Physiology - Heart and Circulatory Physiology* **303**:1273-1282 <https://doi.org/10.1152/ajpheart.00492.2012> | PubMed
67. Sujkowski A., Gretzinger A., Soave N., Todi S. V., Wessells R (2020) Alpha- and beta-adrenergic octopamine receptors in muscle and heart are required for Drosophila exercise adaptations. *PLoS Genet* **16**:e1008778 <https://doi.org/10.1371/journal.pgen.1008778> | PubMed
68. Schiemann R., et al. (2018) Identification and In Vivo Characterisation of Cardioactive Peptides in Drosophila melanogaster. *Int. J. Mol. Sci* **20**:2 <https://doi.org/10.3390/ijms20010002> | PubMed
69. Xie T., et al. (2018) A Genetic Toolkit for Dissecting Dopamine Circuit Function in Drosophila. *Cell Rep* **23**:652 <https://doi.org/10.1016/j.celrep.2018.03.068> | PubMed
70. Mao Z., Davis R. L (2009) Eight different types of dopaminergic neurons innervate the Drosophila mushroom body neuropil: Anatomical and physiological heterogeneity. *Front. Neural Circuits* **3**:612 <https://doi.org/10.3389/neuro.04.005.2009> | PubMed
71. Luan H., Peabody N. C., Vinson C. R. R., White B. H (2006) Refined Spatial Manipulation of Neuronal Function by Combinatorial Restriction of Transgene Expression. *Neuron* **52**:425-436 <https://doi.org/10.1016/j.neuron.2006.08.028> | PubMed
72. Clements J., et al. (2024) NeuronBridge: an intuitive web application for neuronal morphology search across large data sets. *BMC Bioinformatics* **25**:1-25 <https://doi.org/10.1186/s12859-024-05732-7> | PubMed
73. Mais L., et al. (2021) PatchPerPixMatch for Automated 3d Search of Neuronal Morphologies in Light Microscopy. *bioRxiv* <https://doi.org/10.1101/2021.07.23.453511>
74. Wu G., et al. (2024) Opposing GPCR signaling programs protein intake setpoint in Drosophila. *Cell* <https://doi.org/10.1016/j.cell.2024.07.047> | PubMed
75. Liu Q., et al. (2017) Branch-specific plasticity of a bifunctional dopamine circuit encodes protein hunger. *Science* **356**:534-539 <https://doi.org/10.1126/science.aal3245> | PubMed
76. Dana H., et al. (2019) High-performance calcium sensors for imaging activity in neuronal populations and microcompartments. *Nat. Methods* **16**:649-657 <https://doi.org/10.1038/s41592-019-0435-6> | PubMed
77. Men J., et al. (2020) Non-invasive red-light optogenetic control of Drosophila cardiac function. *Commun. Biol.* **3**:336 <https://doi.org/10.1038/s42003-020-1065-3> | PubMed
78. Skora L. I., Livermore J. J. A., Roelofs K (2022) The functional role of cardiac activity in perception and action. *Neurosci. Biobehav. Rev* **137**:104655 <https://doi.org/10.1016/j.neubiorev.2022.104655> | PubMed
79. Koba S., Inoue R., Watanabe T (2016) Role played by periaqueductal gray neurons in parasympathetically mediated fear bradycardia in conscious rats. *Physiol. Rep* **4**:e12831 <https://doi.org/10.14814/phy2.12831> | PubMed
80. Barrios N., Farias M., Moita M. A (2021) Threat induces cardiac and metabolic changes that negatively impact survival in flies. *Current Biology* **0** <https://doi.org/10.1016/j.cub.2021.10.013> | PubMed

81. Neumann J., Hofmann B., Dhein S., Gergs U (2023) Role of Dopamine in the Heart in Health and Disease. *International Journal of Molecular Sciences* **24**:5042 <https://doi.org/10.3390/ijms24055042> | PubMed
82. Ziegler M. G., Kennedy B., Holland O. B., Murphy D., Lake C. R (1985) The effects of dopamine agonists on human cardiovascular and sympathetic nervous systems. *Int. J. Clin. Pharmacol* **23**:175-9 | PubMed
83. Kirouac G. J., Pittman Q. J (2000) A projection from the ventral tegmental area to the periaqueductal gray involved in cardiovascular regulation. *Am. J. Physiol. Regul. Integr. Comp. Physiol* **278**:R1643-50 <https://doi.org/10.1152/ajpregu.2000.278.6.r1643> | PubMed
84. Sato Y., Matsumoto M., Koganezawa T (2024) The dopaminergic system mediates the lateral habenula-induced autonomic cardiovascular responses. *Front. Physiol* **15**:1496726 <https://doi.org/10.3389/fphys.2024.1496726> | PubMed
85. Van Vactor D. L., Cagan R. L., Krämer H., Zipursky S. L (1991) Induction in the developing compound eye of *Drosophila*: Multiple mechanisms restrict R7 induction to a single retinal precursor cell. *Cell* **67**:1145-1155 [https://doi.org/10.1016/0092-8674\(91\)90291-6](https://doi.org/10.1016/0092-8674(91)90291-6) | PubMed
86. Hummel T., Zipursky S. L (2004) Afferent induction of olfactory glomeruli requires N-cadherin. *Neuron* **42**:77-88 [https://doi.org/10.1016/s0896-6273\(04\)00158-8](https://doi.org/10.1016/s0896-6273(04)00158-8) | PubMed

Peer reviews

Reviewer #1 (Public review):

Summary:

This study by Tsuji et al. explores a mechanical threat model in *Drosophila* using air puffs as a stimulus. The authors first establish the paradigm and show that air puffs induce cardiac deceleration along with increased locomotion. They then identify dopamine as a key regulator of this response and go on to map the underlying circuit. In doing so, they pinpoint two pairs of DA-WED neurons as critical players. They carefully used intersectional strategies to achieve relatively clean labeling of these neurons, which helps ensure that the observed effects can be attributed specifically to DA-WED neurons. They further show that DA-WED neurons are both required and sufficient to drive cardiac deceleration, and that their activity increases in response to air puff stimulation. These neurons also contribute to the locomotor response. Directly inducing cardiac deceleration via optogenetic manipulation of cardiomyocytes also increases locomotion, suggesting a link between cardiac state and behavioral output.

Strengths:

Overall, the experiments are thoughtfully designed, well-controlled, and clearly presented. The figures are easy to follow, and the conclusions are generally well supported by the data. The manuscript is also clearly written, with a discussion that acknowledges potential caveats and outlines future directions. The genetic tools, behavioral paradigm, heart rate measurement approaches, and stimulation methods introduced here will be valuable resources for the community.

Weaknesses:

A few minor points to add to the clarity of the manuscript:

(1) The DA-WED driver (R48A08-AD \cap VT008692-DBD \cap TH-FLP) appears quite clean in the brain. However, since the study focuses on cardiac function and locomotion, it would be helpful to check expression in cardiomyocytes and the ventral nerve cord. This would help rule out any off-target expression that might contribute to the phenotypes and further support the idea of a descending pathway from brain dopaminergic neurons.

(2) Since DA-WED>Kir2.1 abolishes the puff-induced locomotor response (Figure 5b), suggesting that DA-WED neurons are directly involved in mediating locomotion. In the model (Figure 5L), it might make more sense for the pathway from mechanical threat to locomotion to pass through DA-WED neurons. The authors could consider adjusting the schematic if they agree.

(3) In line 408, Figure 5K should be 5L as it's a discussion of the model.

(4) In Figure 5j, the x-axis is missing time labels. Even if it matches Figure 5h, adding labels would make it easier to interpret at a glance.

(5) In line 312, it would be helpful to briefly explain why a 28 ms light pulse was used, compared to other pulse durations elsewhere in the paper.

(6) The cardiac deceleration seems to recover quickly after the air puff ends, whereas the locomotor response persists longer (around 10-15 seconds; see Figure 1 and Figure 5). This difference might suggest that DA-WED neurons influence locomotion through an additional or partially independent pathway, beyond their role in cardiac regulation. It could be worth briefly discussing this possibility.

<https://doi.org/10.7554/eLife.111256.1.sa2>

Reviewer #2 (Public review):

Summary:

The authors study cardiac deceleration during threat responses in *Drosophila*. Particularly, it focuses on identifying the neuronal control of this deceleration. Using behavioral and cardiac tracking and analysis, genetics, and calcium imaging, they identify two pairs of dopaminergic neurons involved in cardiac deceleration during air puff responses

Strengths:

The study is overall well done, and the paper is clearly written. Particularly, the work on identifying the two pairs of dopaminergic neurons involved in cardiac deceleration using a series of drivers and generating new ones is rigorous and extensive. Finally, the authors manipulate the heartbeat to investigate how it influences threat responses

Weaknesses:

There are, however, several points that need to be clarified, as some claims are not entirely supported by evidence.

The authors, for example, claim that dopaminergic neurons are responsible for cardiac deceleration (during the air puff, lines 182-3, page 9). However, based on the work in this study, it seems that other neurons could be involved in this control as well. In addition to dopaminergic neurons, the authors test serotonergic and octopaminergic neurons, which, based on silencing experiments, also show an implication in heart-beat deceleration. Furthermore, because they find that dopaminergic neurons are the only ones that, upon thermogenetic activation, lead to lower heart beat frequency, they conclude that the dopaminergic neurons are responsible for air -puff induced cardiac deceleration.

However, these activation experiments are done in a different context than the air puff experiments (at a higher temperature, which could have an effect on the heartbeat changes upon activation of different neuron groups), and because silencing of other monoaminergic neuron types during the air puff also resulted in less cardiac deceleration, one cannot exclude the implication of octopaminergic or serotonergic neurons in air-puff-induced deceleration.

Activation experiments without high temperatures (using, for example, optogenetics) and/or in the presence of the air puff would be important to determine that the dopaminergic neurons are the main type of monoaminergic neurons involved in air-puff-induced cardiac deceleration. Otherwise, the related claims should be rephrased in a way that clearly doesn't exclude a possible implication of other monoaminergic neurons.

Regarding the interactions between the cardiac deceleration and locomotion, the authors propose, based on the results, that the optogenetic cardiac deceleration is sufficient to induce an increase in locomotion, and that it is the decrease in heartbeat that would be responsible via interoceptive pathways to trigger an increase in locomotion. In the model they propose, the DA-WED neurons would induce a decrease in heartbeat that, in turn, would trigger an increase in locomotion. There is not enough proof that cardiac deceleration is the one that triggers an increase in locomotion during air puff responses. As the authors themselves state, the experiments that would demonstrate this would involve preventing cardiac deceleration while optogenetically activating DA-WED. It can therefore not be excluded that the DA-WED neurons trigger an increase in locomotion that is possibly modulated by the cardiac activity. Both alternatives should be considered (models in Figures 4 and 5).

<https://doi.org/10.7554/eLife.111256.1.sa1>

Reviewer #3 (Public review):

Summary:

In this elegant study, Tsuji et al. identify a relationship in *Drosophila* between cardiodynamics and threatening stimuli where mild air puffs elicit a brief bradycardia that coincides with locomotion increases. They then take advantage of the arsenal of genetic tools available in the fruit fly to reveal the indispensability of dopamine, through the action of Dop1R2, in this phenomenon. Further, they pinpoint the source of this dopamine to two specific pairs of neurons - DA-WED that are threat-activated. They then test and find a potential role for cardiac interoception from the heart in linking behavior and cardiodynamics.

Strengths:

This is an interesting and timely story that brings together the tools of fruit fly systems neuroscience and links it with physiology. The experiments are well done and tell a very nice story. In particular, the primary message of the paper - that the authors have identified specific dopaminergic neurons that regulate cardiac activity - is sound.

Weaknesses:

There are no important problems with the scientific approach. Rather, there are some interpretive changes I would consider.

(1) The changes in heart rate are small (10% or so), and, as far as I can tell, are evident for a beat or two. So the data may be better interpreted not as a change in rate but as a lengthening of diastole for a beat or two. That may seem a petty difference, but it might point to particular stretch-activated systems or changes in blood flow as the determinant.

Heart rate must be averaged over time, and so might be blurring the effects. It may be useful to produce figures centered on beat count and duration rather than time. Because the effect may even be just on a single beat, we suggest the authors try plotting the average beat duration for each beat that follows the air puff. If it's really just the first beat, using a quantification of the change of this duration relative to the average that precedes the puff may produce more striking figures.

(2) The author's model that cardiac deceleration leads to walking data is only partially supported by their data. In the first figure, the relationship between cardiac deceleration and walking probability seems to be inverted relative to their model (weak stimulus \rightarrow strong cardiac effect and weak locomotor effect; strong stimulus \rightarrow weak cardiac effect and strong locomotor effect). It is possible that this discrepancy may disappear when the authors look at beat duration rather than heart rate (for instance, if following the strong stimulus, there is a very long beat that is followed by tachycardia, thus weakening their observed HR change). It would also be easier to relate this data in Figure 1 to their interoceptive model if some data were shown that illustrated the relative timing of the cardiac change and the locomotor start.

(3) Also, since the locomotor and cardiac changes are probabilistic, it would be very useful to see how their respective probabilities change when conditioned on the other. According to their interoceptive model, locomotion should preferentially increase on trials where cardiac deceleration occurs. The authors should discuss this incongruity and also potential alternative interpretations of their cardiac manipulation experiments. Perhaps the bradycardia makes them more sensitive to threats - as suggested in the introduction? Control flies show a mild increase in locomotion following green light (Figure 5j), so perhaps by slowing the heart, they are more sensitive and thus respond more strongly to this stimulus?

(4) Looking at the example shapes of the beats in Figure 5g versus Figure 1c, the optogenetically induced diastole has a very different shape from the naturally occurring long beat. Thus, the exact cardiac stimulus may be unnatural. If this is true across trials and animals, it may be worth considering that the funny beat (like an anxiogenic atrial fibrillation in mammals) is the source of the fear and, in turn, locomotor behavior (also interesting!) rather than being a true replication of the cardiac events seen following the puff stimulus.

<https://doi.org/10.7554/eLife.111256.1.sa0>